Journal of Petroleum Science and Engineering 220 (2023) 111247

Contents lists available at ScienceDirect

Journal of Petroleum Science and Engineering

journal homepage: www.elsevier.com/locate/petrol

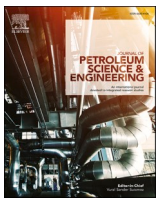

Low salinity water and polymer flooding in sandstone reservoirs: Upscaling from nano-to macro-scale using the maximum energy barrier

Prashant Jadhawar *, Motaz Saeed

School of Engineering, University of Aberdeen, Aberdeen, AB24 3UE, Scotland, UK

ARTICLE INFO

Keywords:
Low salinity waterflooding
Low salinity polymer flooding
Surface complexation modelling
Numerical modelling
Model upscaling

ABSTRACT

In this work, the flooding processes of low salinity waterflooding and low salinity polymer flooding (LSWF and LSP) in sandstone reservoirs were mechanistically modelled at nano-and macro-scales. Triple-layer surface complexation models were utilised to simulate interactions at the oil-brine and sandstone-brine interfaces. The Derjaguin-Landau-Verwey-Overbeek (DLVO) theory was applied to describe the stability of interfacial films in crude oil-brine-sandstone rock systems. The novel application of the maximum energy barrier (MEB), calculated from the interaction potential of the DLVO theory, as an upscaling and interpolant parameter to adjust relative permeability curves as a function of reservoir properties is proposed in this work. Numerical simulations using the commercial simulator CMG-STARS were used in tandem with the surface complexation models and film analysis to evaluate the performance of LSWF and LSP in sandstone reservoirs.

Results of the numerical simulations showed that the LSP gave significantly higher oil recovery compared to standard polymer flooding because of its utilisation of wettability alteration due to LSWF and the improved mobility control due to LSP. A comparison between studied injection processes i.e. low and high salinity waterflooding, and low and high salinity polymer flooding, revealed that oil recovery as a result of wettability alteration is significantly higher than that of mobility control. Further analysis indicated that temperature affects the wettability alteration favourably, and the polymer slug viscosity unfavourably. However, the temperature effect on the wettability was found to be more pronounced. The workflow presented in this study provides valuable guidelines in screening the appropriate sandstone reservoirs for LSWF and LSP applications using the numerical simulation techniques through the upscaling from nano-to-macro-to-field scale.

1. Background

1.1. Overview of low salinity waterflooding

The injection of low-salinity water into reservoirs has been found to improve oil recoveries from reservoirs over the conventional method of reinjecting the formation brine. This has been observed both in laboratory experiments as well as field-scale implementation (Morrow, 1990; Webb et al., 2005; Lager et al., 2008; McGuire et al., 2005; Nasralla and Nasr-El-Din, 2014). This recovery method first gained focus when Morrow and co-authors published their experimental studies on low-salinity waterflooding (LSWF) injection in sandstone cores (Morrow, 1990; Jadhunandan and Morrow, 1991, 1995; Yildiz and Morrow, 1996; Tang and Morrow, 1997; Zhang and Morrow, 2006; Zhang et al., 2007a). Their core flooding experiments showed that reducing the salinity of injected water resulted in higher oil recoveries. Several research studies reported similar effects in both sandstone and carbonate reservoir rocks (Webb et al., 2005; Lager et al., 2008; Nasralla and Nasr-El-Din, 2014; Webb et al., 2004; Lager et al., 2007; Ashraf et al., 2010; Rivet et al., 2010). Incremental recovery of 40% has been detected experimentally from injecting the low-salinity water against the conventional water injection (McGuire et al., 2005). Field trials have also been conducted in sandstone reservoirs: BP's Endicott field in Alaskan North Slope (Seccombe et al., 2008), West and North Semlek, and Moran reservoirs in Minnelusa oil (Robertson, 2007a, 2007b), Omar and Isa fields (Vledder et al., 2010), Snorre oil field (Skrettingland et al., 2011), Burgan Oil field in Kuwait (Abdulla et al., 2013); and the carbonate reservoirs: chalk Ekofisk field located in the Norwegian sector of the North Sea (Austad, 2013), Valhall field in Claire Ridge of UK continental shelf (Barkved et al., 2003; Griffin et al., 2007), an unknown field in Saudi Arabian Upper Jurrasic (Yousef et al., 2012) supported by a number of laboratory investigations.

* Corresponding author.
E-mail address: Prashant.Jadhawar@abdn.ac.uk (P. Jadhawar).

https://doi.org/10.1016/j.petrol.2022.111247
Received 18 July 2022; Received in revised form 5 November 2022; Accepted 10 November 2022
Available online 15 November 2022

Although many studies reported an increased recovery through the injection of ionically modified water, other studies failed to observe such results (Rivet et al., 2010; Sharma and Filoco, 2000; RezaeiDoust et al., 2010; Cissokho et al., 2010). This can be attributed to the fact that the experiments have been conducted in different conditions and using different crude oil, water, and rock samples, which are believed to be the critical factors for the success of the LSWF injection. As a result, many mechanisms have been proposed to be dominant when injecting low-salinity water but no agreement on a certain mechanism has been found yet.

Several mechanisms were proposed as the working mechanism behind the low-salinity effect (LSE) including fines migration, multi-component ion exchange (MIE), pH increase and alkaline-like effect, oil desorption, and electrical double layer expansion among other mechanisms (Lager et al., 2008; McGuire et al., 2005; Austad, 2013; Tang and Morrow, 1999; Buckley and Morrow, 2010; Ligthelm et al., 2009; Zhang et al., 2007b). Fluid-fluid interactions were also proposed as a mechanism for LSWF where the interfacial tension and the surface elasticity may lead to micro-dispersion formation phenomenon and subsequent enhanced oil production (Sohrabi et al., 2017; Tetteh et al., 2021). Lighthelm et al. (Ligthelm et al., 2009) attributed the incremental oil recovery during LSWF to the electrical double layer expansion (DLE). At low or moderate salinities, the thickness of the diffuse layer at the interfaces between rock-brine and crude oil-brine increases with the decreasing ionic strength. This also leads to an increase in the zeta potential at the shear plane which further increases the repulsion between the charged rock surface and the adsorbed polar organic compounds, promoting more water wetting rock conditions. This is consistent with the DLVO (Derjaguin, Landau, Verwey, and Overbeek) theory, which explains that the stability of the colloid is dependent on the balance between the structural, van der Waals attraction, and electrical double layer repulsion forces. Ligthelm et al. (2009), further explained that multi-ion exchange might occur during the process which leads to more decrease in ionic strength. In a critical review of the mechanisms behind the low salinity effect, Jackson et al. (2016a) concluded that the most likely mechanisms are double layer expansion, multi-ion exchange and local increase in pH. Nonetheless, the change in zeta potential and electrostatic forces acting between rock surface and crude oil is a common feature between the three proposed mechanisms. They consequently concluded that zeta potential experiments and evaluation are necessary to understand the role of surface charge in improving oil recovery due to low salinity waterflooding. The work in study will focus on modelling the application of low salinity waterflooding and low salinity polymer flooding in sandstone reservoirs.

1.2. Overview of low salinity polymer flooding

Polymer flooding is an injection of polymer-containing aqueous solution into the reservoir from an injector driving the oil into the producer. The addition of polymer to the injected water increases the viscosity of the displacing (injected) phase which improves the sweeping process resulting in a favourable mobility ratio (Green and Willhite, 1998). Combining the low-salinity waterflooding with polymer flooding utilises the advantage of the wettability alteration induced by LSWF and the improved mobility control resulting from polymer flooding.

The most widely used synthetic polymers are polyacrylamide (PAM) and hydrolysed polyacrylamide (HPAM), while xanthan gum is the most popular natural polymer for EOR applications (Kamal et al., 2015). Hydrolysed polyacrylamide (HPAM) is the most widely used polymer used in enhanced oil recovery mainly due to its good viscosity improvement properties. HPAM polymer rheological properties and adsorption are strongly dependent on brine salinity. Luo et al. (2006) suggested that the polymer viscosity is more sensitive to divalent cations such as Ca^{2+} and Mg^{2+} than monovalent cations i.e. Na^{+}. This is particularly important in polymer flooding and low-salinity polymer flooding, as the targeted dissolved solids for salinity reduction are mainly the divalent cations due to their higher effect on ionic strength and oil adhesion (Lee et al., 2009, 2012; Sheng, 2010; Mandal and Ojha, 2008; Tam and Tiu, 1990).

To predict the viscosity of HPAM polymer solution, the power-law model can be used to describe its pseudoplastic behaviour

$$\mu_p = K\dot{\gamma}^{(n-1)} \quad \text{Eq. 1}$$

where μ_p is the polymer's viscosity in cP, $\dot{\gamma}$ is the shear rate in s^{-1}, K is the flow consistency index and n is the flow behaviour index. The effect of polymer concentration and salinity on the polymer viscosity at zero shear rate, μ_p^0, can be described by the Flory–Huggins equation:

$$\mu_p^0 = \mu_w\left(1 + \left(A_{p1}C_p + A_{p2}C_p^2 + A_{p3}C_p^3\right)C_{sep}^{Sp}\right) \quad \text{Eq.2}$$

where μ_w is the water viscosity, C_p is the polymer concentration, C_{sep} is the effective salinity of the polymer A_{p1}, A_{p2}, A_{p3} and Sp are polymer-specific empirical constants. To calculate the viscosity of HPAM at temperature T based on a known viscosity $\mu_{p,ref}$ at a reference temperature T_{ref} is given as follows (Sheng, 2010)

$$\mu_p = \mu_{p,ref}\ exp\left[E_a\left(\frac{1}{T} - \frac{1}{T_{ref}}\right)\right] \quad \text{Eq.3}$$

where E_a is the activity energy.

Low-salinity polymer flooding (LSP) has been investigated experimentally in different studies. Kozaki (2012) studied the possibility of combining low-salinity waterflooding and polymer flooding through core flooding in Berea sandstone samples. Results showed that injection of low-salinity polymer resulted in a 10% reduction in the residual oil saturation compared to high salinity waterflooding and that the maximum oil recovery was achieved with fewer pore volumes injected. Shiran and Skuage (Shaker Shiran and Skauge, 2013) found that at a low polymer concentration of 300 ppm, LSP incurred very high incremental oil recoveries ranging between 10 and 17% in their coreflooding runs on the Berea sandstone cores.

In carbonate coreflooding, AlSofi et al. (2016) found that the performance of the combined smart water/polymer flooding required significantly lower polymer concentration in comparison with high salinity polymer flooding. The combined process also resulted in 6.5–9.9% additional oil recovery in comparison with the oil recovery expected from the individual processes. Other experimental studies reported that LSP gave incremental oil recovery compared to low and high salinity waterflooding (Jackson et al., 2016b; Saeed et al., 2022a; Brady and Krumhansl, 2012; Brady et al., 2015; Awolayo et al., 2018; Chen et al., 2019; Erzuah et al., 2017).

1.3. Modelling the low salinity waterflooding process

1.3.1. Interactions between crude oil-brine-sandstone rock interfaces during LSWF

Double layer expansion is believed to play a crucial role in reservoir's wettability alteration from oil-wet or weak-water to water-wet conditions. The repulsion between the oil-brine and rock-brine interfaces is dictated by the charges at these interfaces. As the repulsion between the two interfaces increase, the distance between the two interfaces increases leading the oil surface away from the rock surface which enhances the water-wettability in the rock. It has been demonstrated experimentally that improved oil recovery as a result of controlled brine salinity flooding is dictated by the zeta potential and surface charges at the oil and rock surfaces (Jackson et al., 2016b). The interactions within a crude-oil-brine-rock (COBR) system (Fig. 1) are dependent on the oil, brine and rock properties and composition. Studies showed that higher amount of clay minerals such as kaolinite, illite and montmorillonite lead to more positive zeta potential values at the rock-brine interface. And subsequently the wettability of the COBR system becomes less

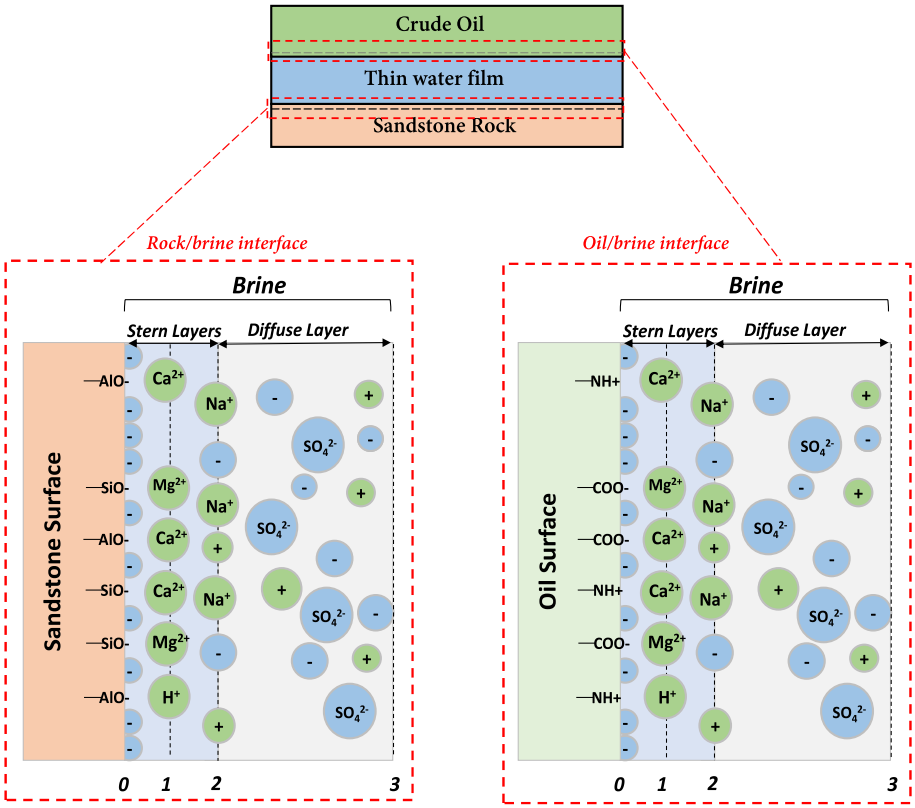

Fig. 1. (top) Representation of thin water film between oil/brine and rock/brine interfaces, (bottom) Representation of the sandstone-brine and oil-brine electrical interfacial layers (Saeed et al., 2022a).

water-wet (Nasralla and Nasr-El-Din, 2014; Saeed et al., 2022a; Brady and Krumhansl, 2012; Brady et al., 2015).

Several surface complexation models (SCMs) has been used to describe the interactions at the oil-brine and sandstone rock-brine interfaces. Most of the developed surface complexation models are diffuse double layer models where the adsorption of the potential determining ions (PDIs) is considered on two electrostatic planes (Brady and Krumhansl, 2012; Brady et al., 2015; Awolayo et al., 2018; Chen et al., 2019; Erzuah et al., 2017; Khalediallidusti and Kleppe, 2018; Pooryousefy et al., 2018; Xie et al., 2017; Sharma and Mohanty, 2018). However, recently triple-layer surface complexation models (TLMs) have been utilised to describe the COBR interactions while accounting for the adsorption of PDIs on three electrostatic planes (Takeya et al., 2019a, 2019b; Bonto et al., 2020; Liu and Wang, 2021; Tetteh et al., 2022a, 2022b; Taheriotaghsara et al., 2021). Our previously developed oil-brine (Saeed et al., 2022b) and sandstone rock-brine (Saeed et al., 2022a) TLMs succeeded in simulating the interactions at both oil-brine and sandstone rock-brine interfaces and were validated against various published experimental datasets. The oil-brine model considered both acidic, –COOH, and basic, –NH, polar surface groups on oil surface. While the sandstone-brine model included both aluminol, >AlOH, and silanol, >SiOH, surface groups on the sandstone surface. The sandstone-brine model also included the crucial individual and collective effects of various sandstone minerals on the overall rock zeta potential. Our previously developed oil-brine and sandstone-brine models (Saeed et al., 2022a, 2022b) are employed in this work to quantify the effects of various parameters on the performances of LSWF and LSP on both nano- and macro-scale levels.

1.3.2. *Interactions between two charged interfaces*

The DLVO theory can be used to calculate the disjoining pressure between two interacting interfaces such oil-brine and sandstone-brine interfaces. The disjoining pressure, $\Pi(h)$, can be calculated as the sum of two repulsive forces, electrical double-layer ($\Pi_{electric}(h)$) and the structural forces ($\Pi_{structural}(h)$), and an attractive force, the van der Waals force ($\Pi_{VdW}(h)$), as follows (Hirasaki, 1991):

$$\Pi(h) = \Pi_{VdW}(h) + \Pi_{structural}(h) + \Pi_{electric}(h) \quad \text{Eq.4}$$

The van der Waals forces can be calculated according to the following equation (Gregory, 1981)

$$\Pi_{VdW}(h) = -\frac{A\left(15.96\left(\frac{h}{\lambda_{lw}}\right)+2\right)}{12\pi h^3\left(1+5.32\left(\frac{h}{\lambda_{lw}}\right)\right)^2} \quad \text{Eq.5}$$

where, λ_{lw} is the London wavelength and can be assumed to be 100 nm (Gregory, 1981), h is the gap between the two plates and A is the Hamaker constant. The structural forces which work in small separation distances between two plates can be calculated by

$$\Pi_{structural}(h) = A_s e^{-\frac{h}{h_s}} \quad \text{Eq.6}$$

where A_s is a coefficient, assumed to be 1.5×10^{10} Pa (Hirasaki, 1991) and h_s is the characteristic length, assigned the value of 0.05 nm (Hirasaki, 1991). The electric double layer forces between two charged plates assuming a constant potential can be given as follows

$$\Pi_{electric}(h) = n_b k_b T\left(\frac{2\psi_{r1}\psi_{r2}\cosh(\kappa h) - {\psi_{r1}}^2 - {\psi_{r2}}^2}{[\sinh(\kappa h)]^2}\right) \quad \text{Eq.7}$$

where n_b is the ion density in the bulk solution, k_b is the Boltzmann constant (1.38×10^{-23}J/K), ψ_{r1} and ψ_{r2} are the reduced surface potentials for the rock-brine and oil-brine interfaces, respectively, and κ is the Debye-Hückel reciprocal length. Further details on calculating the individual forces can be found elsewhere (Hirasaki, 1991; Gregory, 1981; Almansour et al., 2017; Torrijos et al., 2018; Tahir et al., 2018; Unsal et al., 2018; Israelachvili, 2015; Sadeqi-Moqadam et al., 2016).

The aspecific interaction potential energy between two phases interacting through a third phase can also be calculated as follows according to Hirasaki (1991)

$$\omega = \int_{h}^{h_{eq}} \left(\Pi - \Pi_{eq}\right).dh \quad \text{Eq. 8}$$

where h_{eq} and Π_{eq} are the separation distance and disjoining pressure at equilibrium conditions. The maximum of the interaction potential curve or the maximum energy barrier (MEB) reflects the stability of the described colloid or COBR system. This MEB was further utilised by Saeed et al. (2022a) as an indicator of reservoir wettability where the increase in MEB was found to be correlated to an increase in water wettability.

1.4. Numerical modelling of fluid flow in porous media

Reservoir simulators have been developed and applied for several decades to fluid flow in porous media utilising numerical modelling. In this work, advanced and thermal processes commercial simulator CMG-STARS (CMG and STARS User Manual, 2017) is used to simulate the dynamic fluid flow owing to low salinity water and low salinity polymer flooding processes. CMG-STARS has previously been used to model chemical flooding processes such as surfactant-polymer flooding (SayedAkram and Mamora, 2011), polymer flooding (Norris, 2011; Al-Sawafi, 2015), ionic brine flooding and alkaline flooding (Tunnish et al., 2019).

1.4.1. Numerical modelling of low salinity water flooding

One of the earliest works for modelling the LSWF process was carried out by Jerauld et al. (2008). They constructed an analytical and a simulation model to incorporate the salinity effect by modelling the salt as a lumped component. Salinity was directly used as an interpolant between the low and high salinity cases of relative permeability and capillary curves using linear interpolation. A 1D simulation model was developed by Jerauld et al. (2008) to study numerical dispersion (grid resolution). The study shows that grid resolution plays an important part in designing optimum low-salinity water slugs. A similar modelling approach was used by Wu and Bai (2009). However, these studies used only salinity-dependent linear interpolation to change the flow properties which is too simplistic and lacks the appropriate inclusion of any mechanistic mechanisms responsible for LSWF.

Korrani et al. (2016) coupled the geochemical code IPHREEQC with the compositional simulator UTCOMP to model the LSWF by including the geochemical reactions in the process. They used the total ionic strength and the concentration of the organometallic complexes on the surface as interpolants for the relative permeability alteration. They matched the simulation results with core flooding experiments results from BP's Endicott field trial (Lager et al., 2008). Other studies used various types of interpolants such as the weighting function which considered the amount (Ca^{2+}, Mg^{2+}) of divalent cations and desorbed from the mineral surface (Omekeh et al., 2012), Ca^{2+} equivalent fraction on the mineral surface (Dang et al., 2018) among other parameters (Pooryousefy et al., 2018; Sharma and Mohanty, 2018; Korrani et al., 2016; Dang et al., 2018; Qiao et al., 2016); to upscale the nanoscale interactions effect on reservoir wettability to macroscale changes in the relative permeability curves.

In our previous work, the maximum energy barrier concept was utilised as an indicator of reservoir wettability (Saeed et al., 2022a). In this study, the maximum energy barrier is deployed as an interpolant to adjust the relative permeability curves as a function of reservoir conditions, and brine, oil and sandstone composition. Compared to the other scaling parameters, such as salinity, total ionic strength and the concentration of the organometallic complexes, an application of the maximum energy barrier as an interpolation parameter allows the collective inclusion of the effects of temperature, pH and brine, oil and rock composition on the attraction and repulsion forces between the oil and rock. These forces consequently define the oil adhesion to rock surface and COBR system's stability and wettability. Therefore, considering these forces are important in upscaling the LSWF phenomenon from the nano-to-macro-scale. Moreover, the sandstone rock composition and mineralogy has not been considered in previous interpolating parameters. The interpolation process is further explained in the methodology section.

1.4.2. Numerical modelling of low salinity polymer flooding

The modelling of the hybrid processes of combining low-salinity waterflooding and chemical enhanced recovery in general and polymer flooding especially has not been investigated mechanistically thoroughly. Mohammadi and Jerauld (2012) performed several simulations under varying conditions using BP's in-house simulator, VIP; concluding that the use of low-salinity polymer yields an incremental oil recovery in both the secondary and tertiary recovery modes. Khorsandi et al. (2016) developed a model to investigate the synergetic effect of LSWF and polymer flooding through cation exchange reactions using an in-house simulator PennSim. The adsorbed Na^{+} concentration was used as the interpolant for wettability alteration. They concluded that LSWF combined polymer flooding results in higher oil recoveries through favourable alteration of the reservoir wettability. Their model included the effect of divalent and monovalent cations concentration on polymer viscosity. However, the adsorption dependence on salinity and the effects of geochemical reactions on polymer properties were not considered in their simulations. In another work, Khorsandi et al. (2017) developed an analytical model to investigate the LSP process considering cation exchange reactions, wettability alteration, adsorption, inaccessible pore volume and salinity impact on polymer viscosity. They verified their analytical results with experimental data and results from numerical simulation using PennSim. Their work did not consider the effects of geochemical reactions on the polymer properties.

Dang et al. (2018) presented a workflow that utilises a multilayer neural network (ML-NN) to interpolate the effect of the different components such as polymer, salinity, and surfactant on the relative permeability. For the LSW model, they considered different geochemical reactions including aqueous, dissolution, and ion exchange reactions. Scaled ion-exchange fractions were used as interpolants for the wettability alteration model. Their model history matched Alagic and Skauge (2010) experimental results.

The approach used in modelling the combined low salinity water and polymer flooding process adopted in this work is dependent on the wettability and relative permeability alteration process due to LSWF, and polymer flooding (that brings out the sweep efficiency and viscosity improvement). The aim of this study is to present the Maximum Energy Barrier (MEB) as a new interpolating parameter in the relative permeability curves that can be used to upscale low salinity waterflooding and low salinity polymer flooding from nano-scale to macro-scale. This newly developed parameter is then be applied to perform a parametric sensitivity analysis to understand the effects of salinity, temperature, rock mineralogy and type and sequence of injected fluids on the performance of LWSF and LSP. Further details on the approach used in this work is presented in the following section.

2. Methodology

The methodology adopted in this work comprises surface complexation modelling, film stability analysis using DLVO theory and numerical modelling. The surface complexation models utilised in this work are run through PHREEQC, while the numerical modelling was carried out using CMG-STARS for upscaling the crude-oil-brine-rock (COBR) interfacial nano-scale effects embedded in the property Maximum Energy Barrier (MEB) to the macro-scale. The utilised surface complexation model was validated against published experimental studies by comparing the model-predicted zeta potential values with the

experimentally measured values, as presented in the results section. Moreover, the use of maximum energy barrier as an indicator of reservoir wettability was previously validated (Saeed et al., 2022a) and will be discussed again in this work. The LSWF oil recovery predicted through the application of the MEB-interpolated relative permeability curves in the CMG-STARS based numerical modelling has also been validated using the experimental work of Nasralla et al. (2013). The approach developed in this work shall provide valuable understanding to the controlling parameters in LSWF and LSP. Further details on the modelling approach are outlined in the following sections.

2.1. Surface complexation modelling

The oil-brine and sandstone-brine triple-layer surface complexation models (see Fig. 1) used in this work are adopted from our previously reported studies (Saeed et al., 2022a, 2022b). The surface complexation modelling is carried out using the state-of-art geochemical code PHREEQC. The surface complexation reactions included in the utilised model are shown in Table 1. These reactions include the adsorption of various potential determining ions such as H^+, Na^+, Ca^{2+} and Mg^{2+} to oil surface groups, –COOH and –NH, and sandstone rock surface groups, > Al:SiOH. Further details on the adopted TLMs can be found in Saeed et al., 2022a, 2022b.

2.2. Film stability analysis

The film stability analysis in this work is carried out using the DLVO theory. The disjoining pressure and interaction potential are calculated using Eq. (4) and Eq. (8) as a function of the electrostatic double layer (EDL) forces among other factors. The EDL forces are dependent on the zeta potential of the two interacting interfaces i.e. oil-brine and rock-brine interface, which is dependent on the brine, oil and rock composition, reservoir temperature and pH. The zeta potential values at the oil-brine and rock-brine interfaces are calculated using the surface complexation models described in the previous section. Consequently, calculation of the disjoining pressure and interaction potential energy values embedded in the maximum energy barrier (MEB) is determined as the maximum of the interaction potential curve. The relationship (see Fig. 2) between the reservoir's wettability and the maximum energy barrier is then employed in this study as a novel method to interpret the wettability alteration through an adjustment in the relative permeability curves. This is further elaborated in details in the following sections.

2.3. Numerical modelling

The numerical simulations in this research were conducted using the multiphase flow simulator CMG-STARS. First, the approach proposed in this work is validated by history matching the experimental coreflooding results of Nasralla et al. (2013). From the history matching, two sets of relative permeability curves were obtained, one curve corresponds to oil-wet/weak water-wet conditions (high salinity) and another curve corresponds to strong water-wet conditions (low salinity). The history matched relative permeability curves were then used to further validate the proposed approach in this work and run the sensitivity analysis.

A 3D core model with the dimensions 10 × 5 × 10 was constructed in CMG-BUILDER. The grid dimensions were optimised to accurately replicate the core samples sizes used by Nasralla et al. (2013). Rock properties and fluid properties were all constant and the same throughout the grid blocks (refer Table 2). The model was validated by comparing both oil recovery data and pressure drop across the core sample. The same validated model and the set of relative permeability curves were used to run sensitivity analysis to evaluate the effects of salinity, temperature, rock mineralogy and divalent cations on LSWF and LSP. Only difference between the sensitivity and the validated model was the variation in the permeability heterogeneity to better represent real reservoir conditions. The reservoir permeability in the sensitivity model (see Fig. 3) ranged between 10 and 150 mD randomly distributed throughout the core model instead of a homogeneous permeability distribution. Details of the numerical modelling of LSWF and LSP are described below. The base case values and range of sensitivity analysis carried out in this work to achieve the research objectives are summarised in Table 3.

2.3.1. Numerical modelling of low salinity waterflooding: novel approach of MEB as an interpolant for relative permeability curves

The approach used to run each simulation case is illustrated in Fig. 4 in the form of workflow steps. Each simulation case starts by modelling the zeta potential at the oil-brine and sandstone-brine interfaces at the desired reservoir conditions. These calculated zeta potential values are then used to calculate the disjoining pressure and interaction potential between the oil-brine and sandstone-brine interfaces. The maximum energy barrier is then determined from the interaction potential curve. The maximum energy barrier was used as an interpolant to shift the relative permeability curve between oil-wet and water-wet curves. The corresponding upper (MEB_{max}) and lower (MEB_{min}) threshold values of

Table 1
Association/disassociation equilibrium constants, charge distribution and capacitance values optimised in this study for the utilised sandstone-brine and oil-brine TLMs (Saeed et al., 2022a, 2022b).

Surface Complexation Reaction	Log K @ 25 °C	Enthalpy (kJ/mol)	Charge Distribution			C_1 (F/m^2)	C_2 (F/m^2)
			0-plane	1-plane	2-plane		
Sandstone rock-brine surface complexation reactions							
$>AlOH + H^+ \leftrightarrow >AlOH_2^+$	0.8	−5	+1	0	0	2.57	2.57
$>AlOH \leftrightarrow >AlO- + H^+$	−7.5	−40	−1	0	0	2.57	2.57
$>AlOH + Na^+ \leftrightarrow >AlONa + H^+$	−4.5	−60	−1	+0.5	+0.5	2.57	2.57
$>AlOH + Ca^{2+} \leftrightarrow >AlOCa^+ + H^+$	−3.5	−50	−1	+2	0	3.54	2.57
$>AlOH + Mg^{2+} \leftrightarrow >AlOMg^+ + H^+$	−3.5	−50	−1	+2	0	4.92	2.57
$>AlOH + SO_4^{2-} \leftrightarrow >AlO^- + HSO_4^-$	−1.5	–	−1	0	0	2.57	2.57
$>SiOH \leftrightarrow >SiO- + H^+$	−6.5	−40	−1	0	0	2.57	2.57
$>SiOH + Na^+ \leftrightarrow >SiONa + H^+$	−2	−60	−1	+0.5	+0.5	2.57	2.57
$>SiOH + Ca^{2+} \leftrightarrow >SiOCa^+ + H^+$	−2.5	−50	−1	+2	0	3.54	2.57
$>SiOH + Mg^{2+} \leftrightarrow >SiOMg^+ + H^+$	−2.8	−50	−1	+2	0	4.92	2.57
$>SiOH + SO_4^{2-} \leftrightarrow >SiO^- + HSO_4^-$	−1.5	–	−1	0	0	2.57	2.57
Crude oil-brine surface complexation reactions							
$-COOH \leftrightarrow -COO^- + H^+$	−4.7	−60	−1	0	0	2.57	2.57
$-NH + H^+ \leftrightarrow -NH_2^+$	6	73	+1	0	0	2.57	2.57
$-COOH + Ca^{2+} \leftrightarrow -COOCa^+ + H^+$	−3.7	−81	−1	+2	0	3.54	2.57
$-COOH + Mg^{2+} \leftrightarrow -COOMg^+ + H^+$	−4.8	−14.7	−1	+2	0	4.92	2.57
$-COOH + Na^+ \leftrightarrow -COONa + H^+$	−4	−110.5	−1	+0.5	+0.5	2.57	2.57
$-COOH + SO_4^{2-} \leftrightarrow -COO^- + HSO_4^-$	−3.3	–	−1	0	0	2.57	2.57

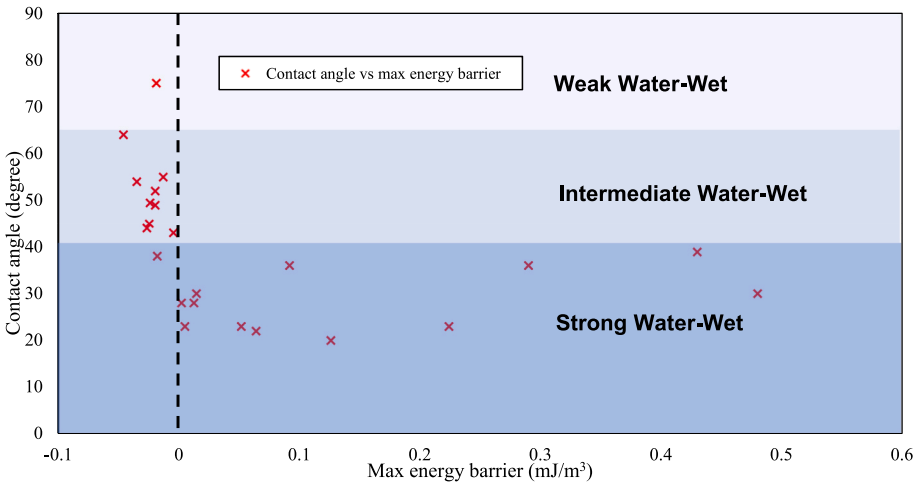

Fig. 2. Correlation between experimentally measured contact angles and calculated maximum energy barrier for each contact angle (Nasralla and Nasr-El-Din, 2014; Xie et al., 2017; Sadeqi-Moqadam et al., 2016; Xie et al., 2014; Lebedeva and Fogden, 2010; Nicolini et al., 2017) (from Saeed et al. (2022a)).

Table 2
Properties of constructed core-scale model for LSWF and LSP simulation in CMG-STARS, adapted from Nasralla et al. (2013)

Property	Value
Number of grids (x,y,z)	(10, 5, 10)
Dimension of grids in cm (x,y,z)	(1.5, 0.747, 0.3735)
Porosity	0.19
Permeability (mD)	80.9–95.4
Oil viscosity at 100 °C (cP)	2.6
Water viscosity at 100 °C (cP)	0.28
Initial core pressure (kPa)	500

the maximum energy barrier correspond to low salinity and high salinity cases, respectively. At an energy barrier above MEB_{max}, the system is assumed to be always strong water-wet and below MEB_{min} the system is weak water-wet/oil-wet. The minimum and maximum MEB values are determined based on the experimentally derived relative permeability curves corresponding to weak water-wet and strong water-wet systems, respectively.

In this paper, these values are based on the experimental work of Nasralla et al. (2013) as discussed in the results section. An energy barrier above MEB_{max} the system is characterised as a stable system where the oil-brine interface repels the rock-brine interface leading to a stronger water-wet system. The adjustment of the relative permeability curve was carried out by linearly interpolating the endpoint values of the relative permeability curves as a function of the maximum energy barrier interpolant as depicted in Fig. 5. The interpolation process was carried out by first calculating a weighting parameter, θ, as a function of the maximum energy barrier:

$$\theta = \frac{MEB - MEB_{min}}{MEB_{max} - MEB_{min}} \quad \text{Eq. 10}$$

where MEB is the current maximum energy barrier, MEB_{min} is the lower limiting case of the maximum energy barrier and MEB_{max} is the upper limiting case of the maximum energy barrier determined from the experimentally derived relative permeability curves. Using the calculated weighting factor, the altered relative permeabilities and residual oil saturation can be calculated as follows:

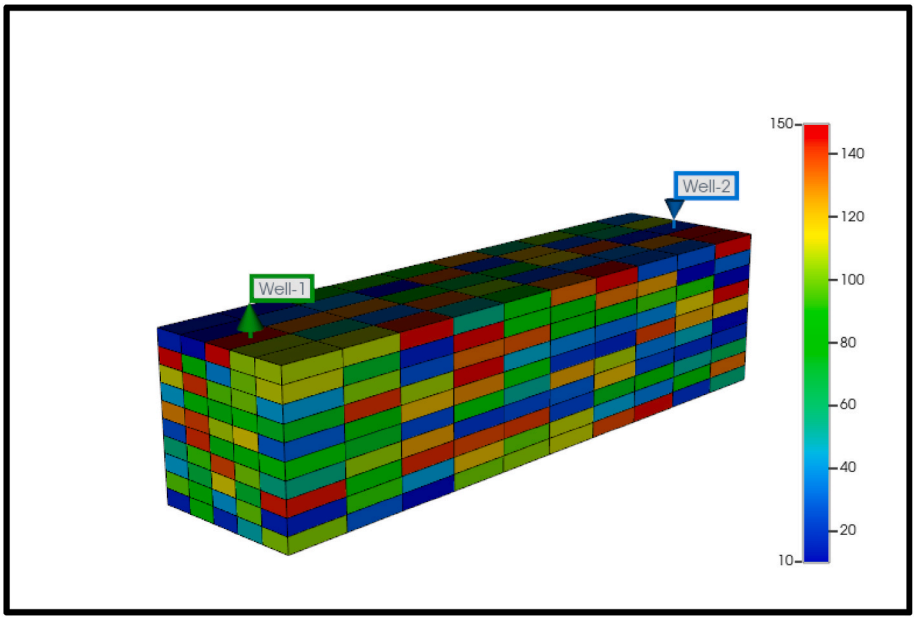

Fig. 3. Distribution of permeability (mD) in the core-scale simulation model for LSWF and LSP simulation in CMG-STARS.

Table 3
Base case values and range of parameters used for sensitivity analysis for LSWF and LSP.

LSWF Cases				
Sensitivity parameter	Base Case	Low	High	
Average (>Al:SiOH) site density (site/nm^2)	*2.5*	*0.6*	*5.5*	
TAN	*0.5*			
TBN	*0.5*			
Temperature (°C)	*60*	*40*	*80*	
pH	*7*			
Salinity (mol/L)	*0.5*	*0.5*	*2*	
Electrolyte	*NaCl*			
LSP Cases				
Sensitivity parameter	**Base Case**	**Low**	**High**	
Average (>Al:SiOH) site density (site/nm^2)	*2.5*			
TAN	*0.5*			
TBN	*0.5*			
Temperature (°C)	*60*	*40*	*100*	
pH	*7*			
Salinity (mol/L)	*0.5*	*0.5*	*3*	
Electrolyte	*NaCl*			
HPAM concentration (ppm)	500 ppm			
Type of process	*LSPF*	*LSWF*	*HSPF*	*HSWF*

$$k'_{rw} = \theta \times k^{ww}_{rw} + (1-\theta) \times k^{ow}_{rw} \quad \text{Eq. 11}$$

$$k'_{ro} = \theta \times k^{ww}_{ro} + (1-\theta) \times k^{ow}_{ro} \quad \text{Eq. 12}$$

$$S'_{orw} = \theta \times S^{ww}_{orw} + (1-\theta) \times S^{ow}_{orw} \quad \text{Eq. 13}$$

where k_{rw}, k_{ro} and S_{orw} are the water relative permeability, oil relative permeability and residual oil saturation, respectively. The superscripts "' ", "ww" and "ow" denote altered, water-wet and oil-wet values, respectively. The curvature of the relative permeability curves is essentially dictated by the capillary pressure inside the core plug sample, however, in these simulation models the effect of change in capillary pressure is neglected. The interpolated relative permeability curves are then adopted in the constructed model to simulate the flow conditions within the COBR system in each studied case.

2.3.2. Numerical modelling of low salinity polymer flooding

To simulate the LSP cases, the approach detailed in Fig. 6 was adopted. It starts by modelling the zeta potential of the oil-brine and rock-brine interfaces. Disjoining pressure and interaction potential were then calculated by adopting the calculated zeta potential values. The maximum energy barrier between the oil-brine and rock-brine interfaces is then quantified and used as an interpolant for the relative permeability curves, as per the stated approach in section 3.3.1. The polymer solution viscosity was calculated using the correlations Eq. (1), Eq. (2) and Eq. (3). Relative permeability curves and polymer solution viscosity were calculated independently of each other. In all the simulated polymer cases, a 0.2 PV of polymer slug is injected after 1.2 PV of water followed by 0.6 PV of water.

3. Results and analyses

3.1. Validation of triple-layer surface complexation models

The oil-brine (Saeed et al., 2022b) and sandstone-brine (Saeed et al., 2022a) TLMs adopted in this work were validated against experimental data from literature by comparing the zeta potential values from the models with the experimentally measured values. The validation for the oil-brine TLM was performed against 9 published studies (Nasralla and Nasr-El-Din, 2014; Pooryousefy et al., 2018; Takeya et al., 2019a; Takeya et al., 2019b; Nasralla et al., 2013; Buckley et al., 1989; Kolltveit, 2016; Ayirala et al., 2018; Yang et al., 2016) with 16 different types of crude oils. A comparison between the model-predicted and experimentally measured zeta potential for Moutary and Leduc (Buckley et al., 1989) crude oils at 0.1, 0.01 and 0.001 M NaCl is shown in Fig. 7. The model was successful in predicting the zeta potential for two types of crude oil at varying ionic strengths compared to experimental data. More validation analysis of adopted oil-brine TLM can be found elsewhere (Saeed et al., 2022b). The sandstone-brine TLM was also validated against experimental data from 8 different studies using rock samples with varying mineralogy and experimental conditions. Fig. 8 exhibit the comparison between zeta potential values predicted form the adopted sandstone-brine TLM and two experimental studies (Farooq et al., 2011; Alotaibi et al., 2011) for Berea sandstones and Scioto sandstone. The comparison show that the model was able to predict the zeta potential at the rock-brine interface with accuracies ranging from 69% to 97%. Although, the accuracy is not high at some points, this model remains the only to include the individual and collective effects of clay minerals on the rock-brine zeta potential as far as we know. Additional validation comparisons are detailed by Saeed et al. (2022a).

3.2. Numerical modelling of LSWF: replicating Nasralla et al. (2013) coreflooding results

The LSWF coreflooding results reported by Nasralla et al. (2013) were used to validate the approach described in 3.3. Brines with four salinities (deionized water, aquifer water, formation water and sweater) (see Table 4) were injected into a sandstone core samples and the oil recovery was recorded. The history matching was carried out using the model described in Table 2 with a homogeneous reservoir permeability ranging from 80.2 mD in DIW case to 95.4 mD in the SW case. Due to the absence of relative permeability data in the work of Nasralla et al. (2013), we first history-matched the limiting cases of oil recovery (highest and lowest) by altering the relative permeability endpoints to tune with the coreflooding performance. The highest oil recovery was reported from using deionized water and the lowest recovery from using seawater. Consequently, the MEB was calculated for the two limiting cases to determine the interpolation limiting values of MEB for the relative permeability curves. The data required for the MEB calculations was adapted from Nasralla et al. (2013), After that the MEB values for the two intermediate cases, i.e. formation water and aquifer water, were calculated and used as interpolating values to calculate the relative permeability curves between the two limiting cases. The limiting high MEB value in the deionized water case was found to be 1.65 mJ/m^2 and the limiting low MEB value in the seawater was −0.0147 mJ/m^2. The MEB for the intermediate salinity cases, FW and DIW, were −0.01 mJ/m^2 and 1.08 mJ/m^2, respectively. Using the MEB as an interpolant, the interpolated relative permeability curves for the FW and DIW cases were obtained. The history matched and interpolated relative permeability curves for the four cases used for validation are shown in Fig. 9. The comparison of the oil recovery predicted from the proposed approach in this work against the experimentally reported oil recovery is shown in Fig. 10a. Moreover, the pressure drop observed in the coreflooding experiments for the deionized water case was history matched using the developed model as exhibited in Fig. 10b. It can be seen from the comparison that the history matching of the two limiting cases' oil recoveries: deionized water (DIW) and seawater (SW), and the prediction of the two intermediate cases' recoveries: formation water (FW) and aquifer water (AQ), were successful. Hence, we believe that the approach proposed in 3.3. can be used to upscale nanoscale interactions to core-scale flow phenomena successfully.

3.3. Sensitivity analysis of LSWF oil recovery

3.3.1. Effect of NaCl salinity

The effect of NaCl salinity on the low-salinity waterflooding in a core

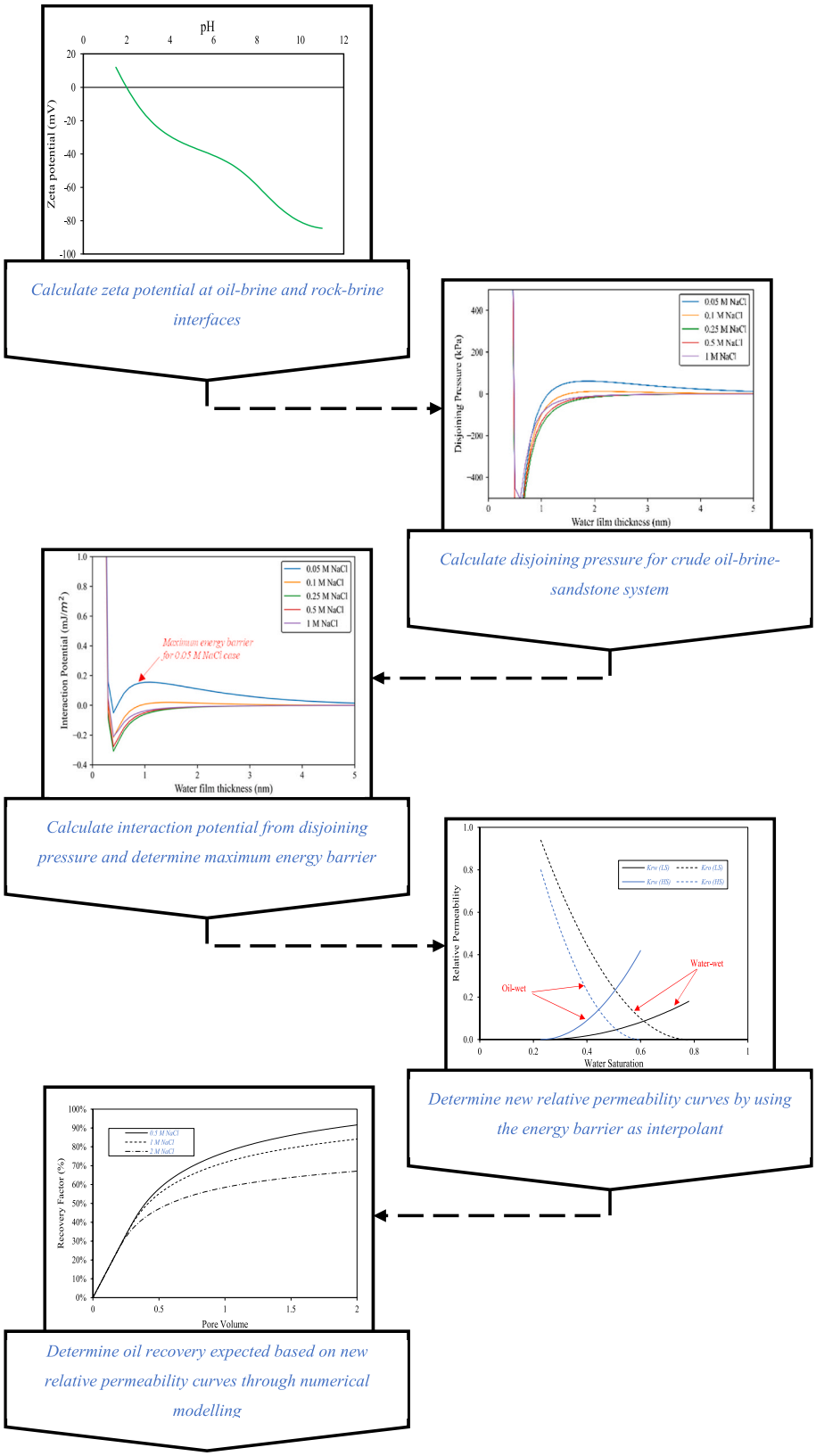

Fig. 4. Workflow to numerically simulate the low-salinity waterflooding (LWSF) cases.

scale model was assessed. The investigated water salinities are 0.5 and 3 M NaCl at 60 °C. The zeta potential was first predicted for both oil-brine and rock-brine interfaces at the desired salinities as shown in Fig. 11. The predicted zeta potential curves show that the zeta potential become less negative as the salinity increases where oil-brine (OB) salinity was −30 mV at 0.5 M NaCl and −5 mV at 3 M NaCl. Subsequently, the disjoining pressure curves, and interaction potential curves were calculated for each salinity case as depicted in Fig. 12. Both disjoining

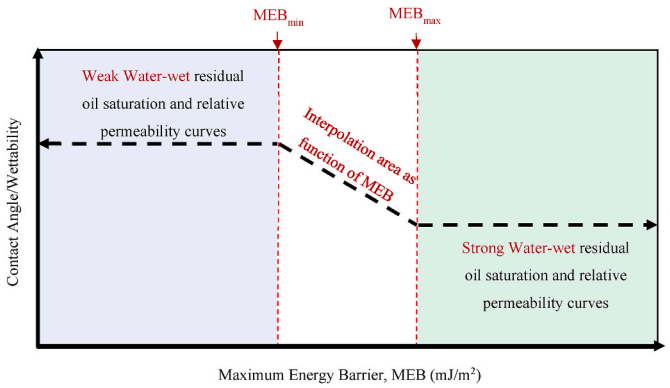

Fig. 5. MEB Interpolation curve between weak water-wet and strong water-wet residual oil saturations and relative permeability curves.

pressure and interaction potential curves shift lower as the brine salinity increases, reflecting a decrease in the COBR system stability. Details of the calculated zeta potential values and MEB for each studied case is given in Appendix A. Firstly, the effect of salinity on the relative permeability is evaluated as shown in Fig. 13a. It can be seen that the relative permeability curve of 0.5 M NaCl salinity case reflects more water-wet conditions in comparison with the 3 M NaCl case. Also, the lower salinity of 0.5 M NaCl resulted in a lower residual oil saturation of 0.22 and the oil phase flows with more ease in comparison with the other salinity case i.e., 3 M NaCl. These improved oil flow properties have been translated to oil recovery terms as depicted in Fig. 13b, where 0.5 M NaCl salinity incurred a higher oil recovery of 38.35% followed by 3 M NaCl which resulted in a lower oil recovery of 34.1%. The same observation can be made from Fig. 13c where the oil rate and water cut data are depicted. The water cut of the high salinity case of 3 M NaCl increases faster with the injected pore volume leading to the earlier water breakthrough resulting in lower oil production in comparison with 0.5 M NaCl salinity.

Results shown in Fig. 13 highlight the objective of low-salinity waterflooding where a decrease in the water salinity results in an increase in the oil production. This can be explained by the higher repulsion expected between the oil and sandstone surfaces when the salinity is reduced. The decrease in salinity results in a direct depletion of the positive Na^+ ions present in the brine leading to higher negative surface charges on both oil and sandstone surfaces resulting in an enhanced repulsion between the two surfaces. The higher the repulsion, the sandstone rock becomes more water-wet and oil adhesion is reduced. Consequently, the residual oil saturation in the 0.5 M NaCl, 0.32, is lower than that of 3 M NaCl, 0.35. This is also reflected in the overall relative permeability curves where lower salinities result in the oil phase passing through pores with more ease than the higher salinity cases. As a result, the overall oil recovery (see Fig. 13a) improved as the water salinity decreased with a 4.3% incremental oil recovery expected between the low and high salinity cases. This signifies the importance of LSWF in improving the oil recovery from sandstone reservoirs.

3.3.2. Effect of divalent cations

Saeed et al. (2022a) reported that the presence of divalent cations in the formation water leads the sandstone reservoir wettability to be less water wet in comparison with the monovalent cations. In this section, the role of the divalent cations is evaluated in terms of relative permeability, oil recovery and fluid production. Two brines with the same salt concentration, 0.5 M, are used for the comparison, one is NaCl and the other is $CaCl_2$. The relative permeability curves plotted by linearly interpolating the predicted MEB between the oil-wet and water-wet cases are depicted in Fig. 14a. The NaCl salt resulted in a significantly lower residual oil saturation of 0.32 in comparison with 0.35 residual oil saturation in the case of $CaCl_2$ salt. The relative permeability curve of the NaCl salt reflects more water-wet conditions in contrast to the $CaCl_2$ salt case which corresponds to weaker water-wet conditions. The predicted oil recovery is plotted against the injected pore volumes in Fig. 14b shows that NaCl salt case resulted in 4.4% incremental oil recovery over the $CaCl_2$ salt case. The oil production drops faster as the pore volume increases in the case of $CaCl_2$ salt case compared to the NaCl case.

The presence of the divalent Ca^{2+} cation in the formation brine leads to a higher screening of the negative surface charges on both the oil and sandstone surfaces. This leads to less repulsion between the oil and rock surfaces resulting in an increase in the oil adhesion to the sandstone rock hence promoting oil wetting conditions. This is indicated in the relative permeability curves in Fig. 14a as the $CaCl_2$ salt led to higher residual oil saturation of 0.35 in comparison with that of NaCl salt i.e. 0.32. This difference in the relative permeability curves is reflected in the predicted oil recovery of waterflooding for the two cases, as the NaCl salt provided higher oil recovery than that of the $CaCl_2$ case. The use of NaCl injection brine, as opposed to CaCl2 brine, resulted in a slower production of water, indicated by water cut in Fig. 14c, from the reservoir which led to higher overall oil production. Results discussed in this section indicate that divalent cations should be removed from the injection water prior to the flooding process to improve the performance of waterflooding in sandstone reservoirs.

3.3.3. Effect of temperature

The impact of reservoir temperature on the waterflooding performance is investigated at three temperatures 40, 60 and 80 °C in 0.5 M NaCl salinity brine and crude oil whose TAN = TBN = 0.5 mg KOH/g. The effect of temperature on the relative permeability curves is illustrated in Fig. 15a, where the 80 °C case exhibits stronger water wetting conditions in comparison with the 40 and 60 °C curves. The oil recovery expected from the three cases of temperature is plotted in Fig. 15b against the injected pore volumes. Oil recovery at 80 °C is significantly higher than that at 40 and 60 °C. A total of 8.2% incremental oil recovery is expected in the 80 °C case compared to the 40 °C case. The oil production and water cut are also evaluated for the three studied cases as shown in Fig. 15c where the oil production in the 40 and 60 °C cases drops faster than that of the 80 °C case allowing for more oil production.

The increase of sandstone reservoir temperature enhances the deprotonation of the surface groups present on both oil and sandstone surfaces i.e. –COOH, –NH, >AlOH and >SiOH, leading to more negatively charged surface groups. This increases the negative surface charges on both oil and rock surfaces which boosts the repulsion between the two surfaces leading to higher oil release from the rock surface. Consequently, at higher temperatures the relative permeability curves (see Fig. 15a) exhibit stronger water wet behaviour compared to the lower temperatures. The residual oil saturation at 80 °C is 0.2 while the residual oil saturation at 40 °C is 0.35 which highlights the higher oil adhesion at a lower temperature. Furthermore, the oil recovery (Fig. 15b) expected from a waterflooding process in a sandstone reservoir/core is strongly dependent on the temperature of the reservoir/core. Increasing the temperature from 40 °C to 80 °C resulted in an incremental oil recovery of 8.2%. The water cut data plotted in Fig. 15c shows that the higher temperature delays the water breakthrough and reaching the 98% water cut beyond which the oil well usually becomes uneconomical to produce from. Results discussed in this section revealed that reservoir temperature plays an important role in dictating the performance of waterflooding. It is also highlighted that the oil production is enhanced as the reservoir temperature increases, hence, hot water should always be considered instead of water at surface temperature for waterflooding and low-salinity waterflooding processes in sandstone reservoirs. Because cold waterflooding and low-salinity waterflooding may result in an unfavourable reversal in sandstone wettability from strong water-wet to weak water-wet conditions cancelling the desired low-salinity effect.

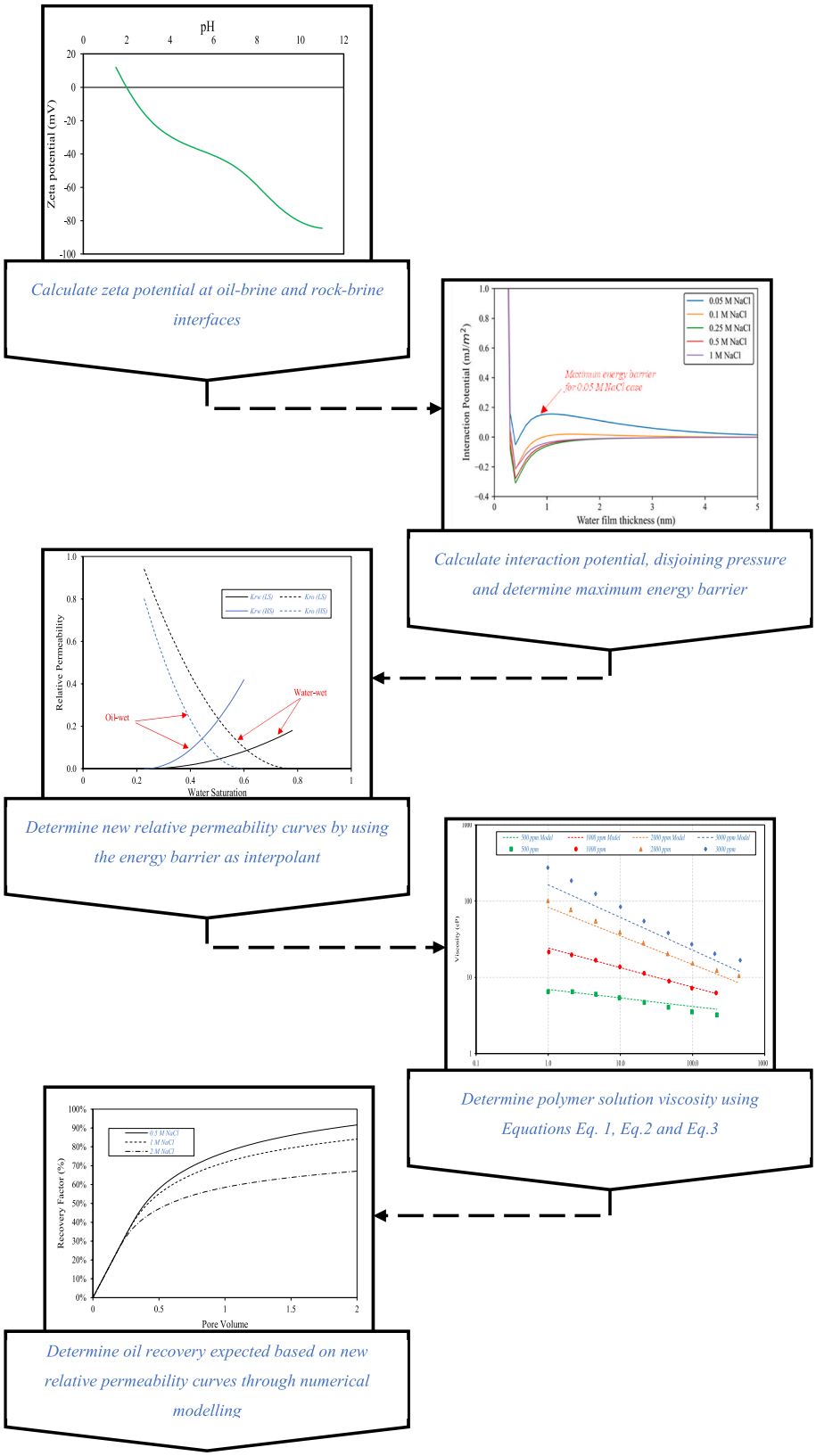

Fig. 6. Workflow to numerically simulate the low-salinity polymer flooding cases.

3.3.4. *Effect of average rock site density*

The mineralogical composition of the sandstone rock impacts reservoir wettability. The performance of a waterflood is dependent on the reservoir's wettability and hence on rock mineralogy. In this section, the impact of rock mineralogy and average rock site density on the waterflood performance is assessed. To highlight the impact of varying average rock site density, the base case brine salinity used in this investigation is 0.5 M NaCl. The impact of rock mineralogy is

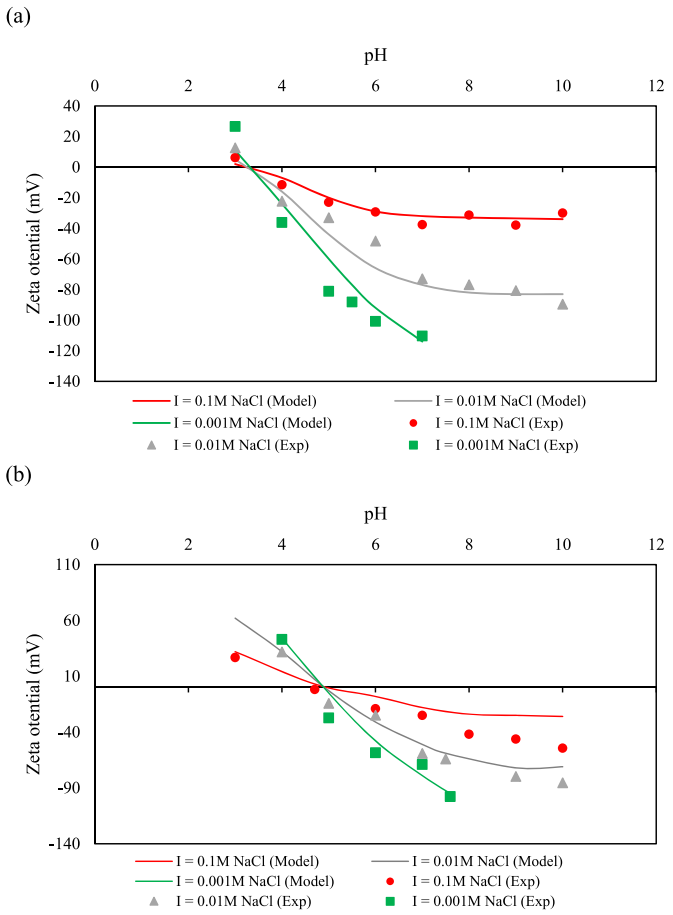

Fig. 7. Experimental and modelling zeta potential values for (a) Moutray crude oil and (b) Leduc crude oil (experimental results from Buckley et al. (1989); Saeed et al. (2022b).

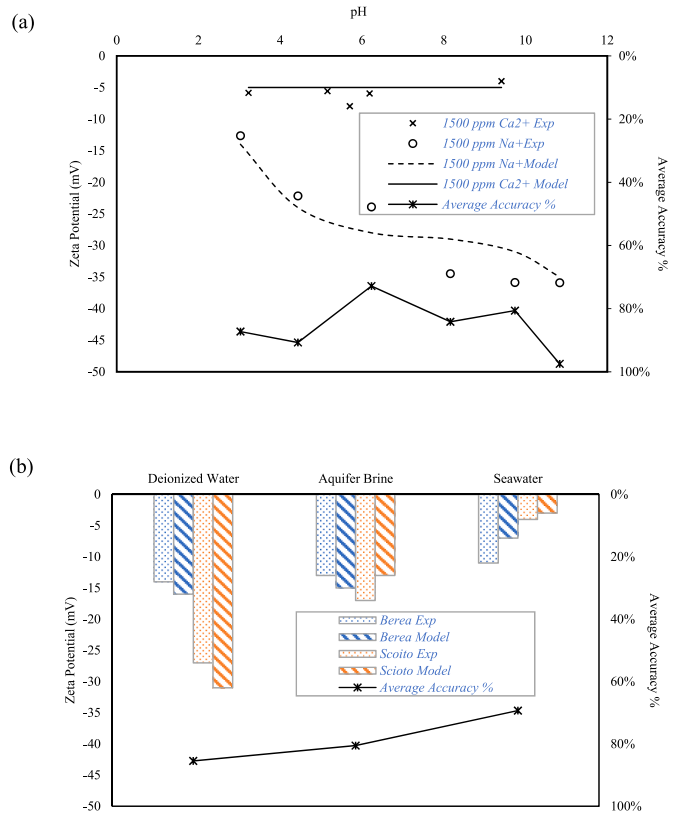

Fig. 8. Experimental and modelling zeta potential values for (a) Berea sandstone (Farooq et al., 2011) *and* (b) Berea sandstone sample and Scioto sandstone sample (Alotaibi et al., 2011; Saeed et al. 2022a).

investigated for average rock site density values 2.5 and 5.5 site/nm^2. Fig. 16a shows the altered relative permeability curves for the two studied cases, 2.5 and 5.5 site/nm^2. It can be seen that the relative permeability curve for the lower site density is shifted to the right compared to the higher site density 5.5 site/nm^2. This indicates that the lower site density results in more water wetting conditions. The overall predicted oil recovery expected from the waterflood in the two studied cases is depicted in Fig. 16b. Lower rock site density resulted in higher oil recovery compared to the higher site density of 5.5 site/nm^2. An incremental oil recovery of 2.8% is expected in the 2.5 site/nm^2 case over the 5.5 site/nm^2 case. The oil production rate (Fig. 16c) predicted from a sandstone rock with a 2.5 site/nm^2 reaches a peak of 0.5 cc/min and declines slower than that from a rock with 5.5 site/nm^2. Consequently, the water cut predicted from a 5.5 site/nm^2 sandstone rock increases slightly faster as the production continues compared to the water cut expected from the 2.5 site/nm^2 rock.

The average rock site density controls the number of sites available on the rock surface for the brine's positively charged cations to adsorb on. This leads to higher adsorption of positively charged ions to the rock surface resulting in a reduction in the negative surface charge formed at the rock surface. As a result, the repulsion expected between the oil and rock surfaces is reduced allowing for more oil to adhere to the rock surface. Hence, the COBR system becomes more oil-wet. This is reflected in the relative permeability curves in Fig. 16a, where the rock with the higher surface site density is more oil-wet compared to the rock with a lower surface site density of 2.5 site/nm^2. Therefore, the residual oil saturation in the case of 5.5 site/nm^2 site density is 0.34 which is higher than that of the 2.5 site/nm^2 site density i.e. 0.24. This is because the crude oil adheres more to the rock surface in the case of higher clay content and higher average site density as depicted in Fig. 17. The shift in the relative permeability curves is projected on oil recovery predicted from the waterflooding performance in the two studied cases, 2.5 and 5.5 site/nm^2 as illustrated in Fig. 16b. The oil recovery expected from a waterflood from a 2.5 site/nm^2 rock is 2.8% higher than that expected from a 5.5 site/nm^2 rock due to the ease of the oil flow through the low site density rock. Therefore, it is important to evaluate the rock mineralogy of the sandstone reservoir when designing a low-salinity waterflooding.

Table 4
Water chemistry of different brine used in coreflooding experiments used by Nasralla et al. (2013)

Ions	Concentration (mg/L)		
	FW	SW	AQ
Na^+	54,400	16,877	1504
Ca^{2+}	10,600	664	392
Mg^{2+}	1610	2279	66
Sr^{2+}	–	–	5
Cl^-	170,000	31,107	2577
HCO_3^-	176	193	192
SO_4^{2-}	370	3560	700
TDS (mg/L)	174,156	54,680	5436

3.4. Numerical modelling of low salinity polymer flooding: sensitivity of oil recovery

3.4.1. Effect of salinity

Salinity affects both reservoir wettability and the viscosity of the HPAM polymer solution. The impact of salinity on the hybrid low-

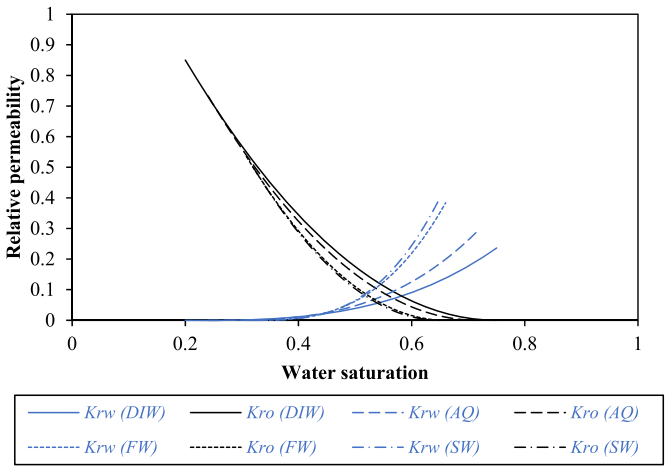

Fig. 9. History matched deionized water (DIW) and seawater (SW), and MEB-interpolated aquifer water (AQ) and formation water (FW) relative permeability curves. History matched to results of Nasralla et al. (2013).

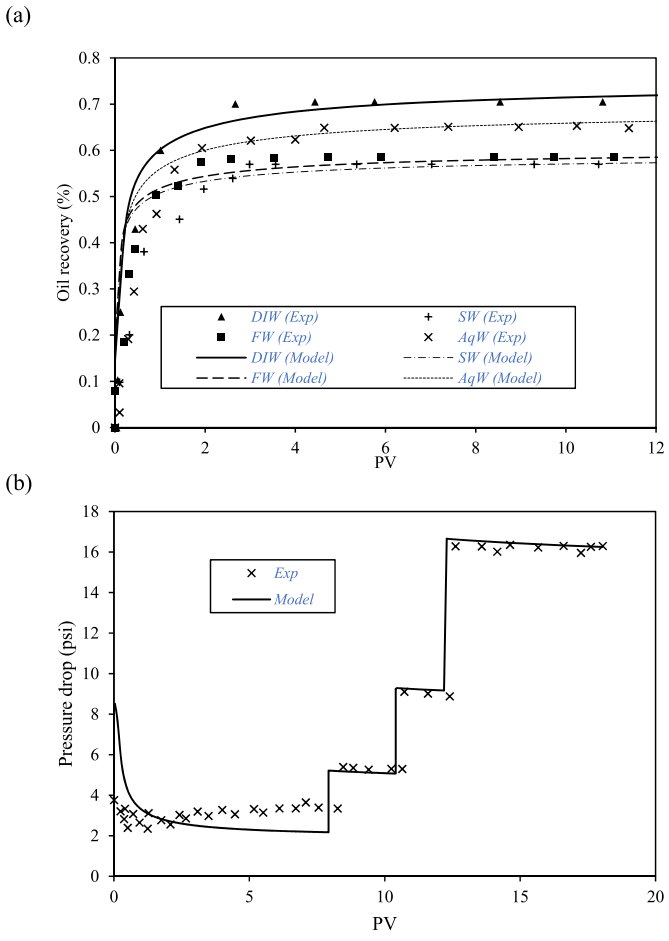

Fig. 10. History matching and validation of (a) oil recovery data and (b) pressure drop of deionized water flooding as reported by Nasralla et al. (2013).

salinity polymer flooding process is evaluated at salinities 0.5 and 3 M NaCl. A comparison between the oil recoveries expected from each injected fluid salinity is shown in Fig. 18a and b. It can be seen that the oil recovery predicted from injecting the 0.5 M NaCl fluid is significantly higher than injecting 3 M NaCl salinity fluid. An incremental oil recovery of 4.7% is observed from 0.5 M NaCl fluid compared to 3 M NaCl fluid. It can also be seen from Fig. 18a that the oil recovery increases as

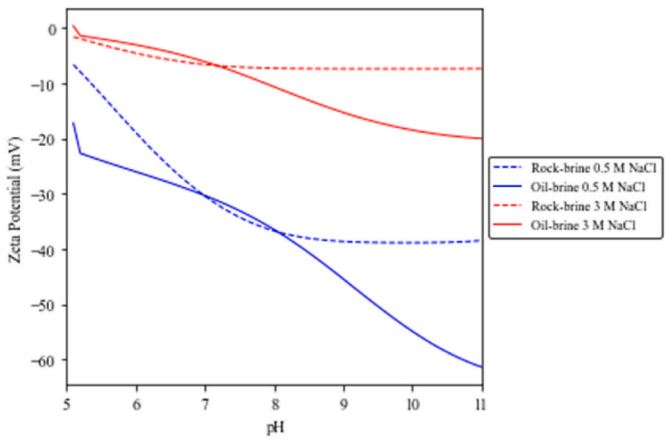

Fig. 11. Zeta potential curves for oil-brine and rock-brine interfaces at 0.5, 1 and 3 M NaCl.

the salinity of the injected brine is reduced. Fig. 18c shows the water cut and oil production expected from each injected fluid, where the 0.5 M NaCl salinity fluid gave significantly lower water cut compared to 3 M NaCl.

Salinity affects the low-salinity polymer flooding process by affecting both the reservoir's wettability and solution viscosity. As discussed in section 4.2.1, the reduction in the brine salinity results in shifting the reservoir wettability into more water wetting conditions resulting in higher oil recovery. Brine salinity plays a vital role in dictating the polymer's viscosity. Increasing the brine salinity leads to increased screening of the negative charges present on the HPAM polymer chains. This reduces the repulsion between the polymer chains causing them to coil reducing the effective viscosity of the polymer. Therefore, increasing the injected fluid salinity leads to a reduction in the viscosity of the injected polymer slug. This is interpreted in Fig. 18a and b where the increase in brine salinity resulted in lower oil recovery. The calculated polymer viscosity and relative permeability curve endpoints for each case is give in Appendix A. Another observation is that after injecting the polymer slug, a rapid increase in the oil recovery is observed. A similar observation can be made in Fig. 18c where a rapid increase in oil produced compared to water production is evident. This can be explained by the fact that the polymer slug improves the mobility ratio between the aqueous phase and the oil phase, by reducing the water mobility. The effect of salinity on the polymer viscosity can particularly be seen by examining the oil production rate and water cut (Fig. 18c) for the 0.5 M NaCl. In the pore volume range between 1.2 and 1.4, for the 0.5 M NaCl fluid the water cut drops from 97% to 94%, which is not observed in the case of 3 M NaCl. This is a result of the higher viscosity exhibited by the 0.5 M NaCl polymer slug compared to the 3 M NaCl slug. This realisation highlights the critical role of the injected fluid salinity in the performance of polymer flooding in general and why low-salinity polymer flooding should always be considered for an improved flooding performance.

3.4.2. *Effect of temperature*

As discussed previously in 4.2.4, elevated temperatures cause the reservoir wettability to be more water-wet which aids in recovering more oil. In this section, the impact of temperature on the performance of low-salinity polymer flooding is evaluated at 40, 60 and 100 °C. The oil recovery expected from 0.5 M NaCl LSP in a sandstone reservoir at various temperatures is shown in Fig. 19a and b. At 40 °C, the expected oil recovery from LSP was 34.4%. When the temperature was increased to 100 °C the oil recovery significantly increased to 51.1%.

The effect of temperature on the low-salinity polymer flooding process is a contradicting one because the increase in temperature results in a favourable shift in the reservoir wettability and an unfavourable shift

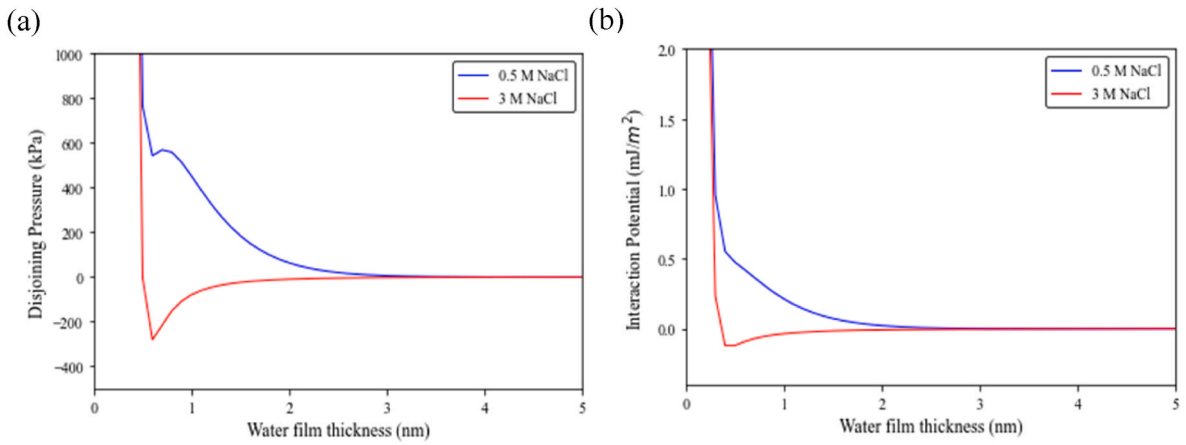

Fig. 12. (a) Disjoining pressure curve and (b) Interaction potential energy curve at 0.5, 1 and 3 M NaCl salinities.

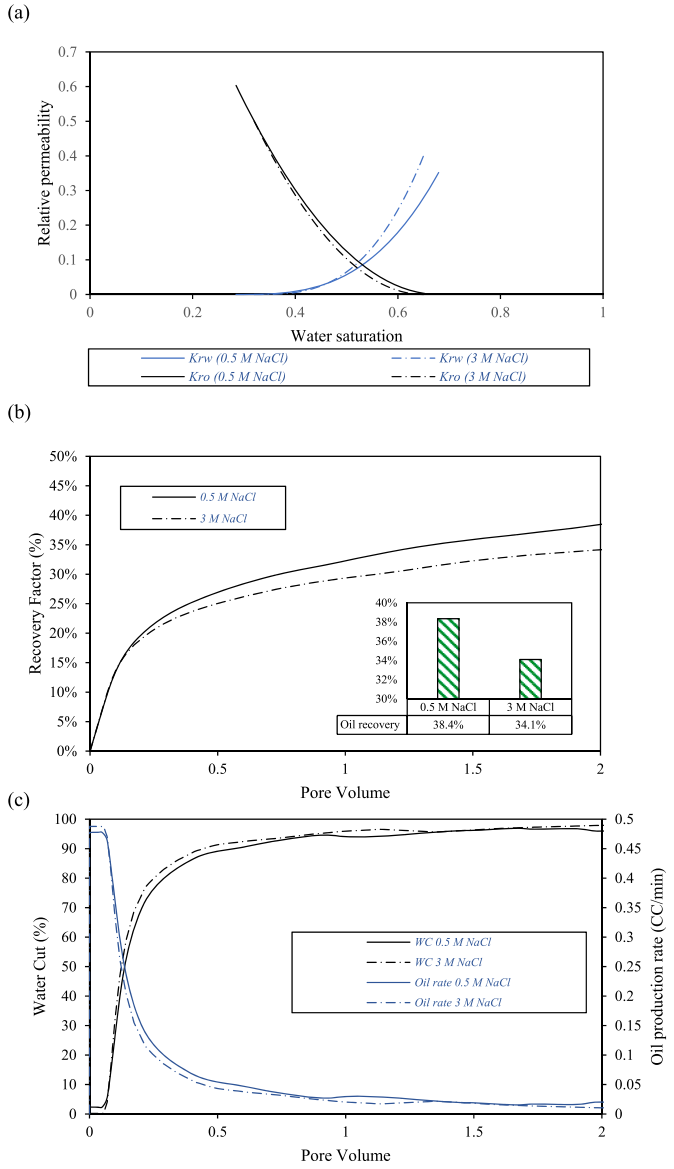

Fig. 13. (a) Relative permeability curves (adjusted for salinity using MEB based on history matched curves to results from Nasralla et al. (2013), (b) oil recovery profile and (c) oil production and water cut profiles for 0.5, 1 and 3 M NaCl waterflooding cases.

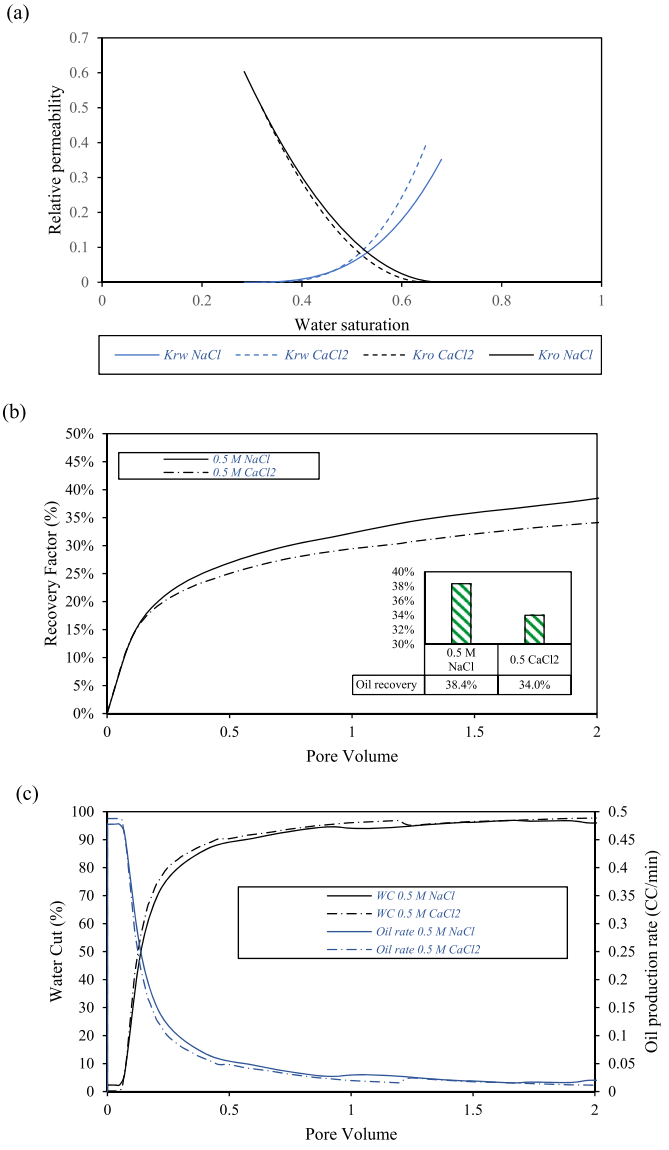

Fig. 14. (a) Relative permeability curves (adjusted for salinity using MEB based on history matched curves to results from Nasralla et al. (2013)), (b) oil recovery profile and (c) oil production and water cut profiles for 0.5 M NaCl and 0.5 M $CaCl_2$ waterflooding cases.

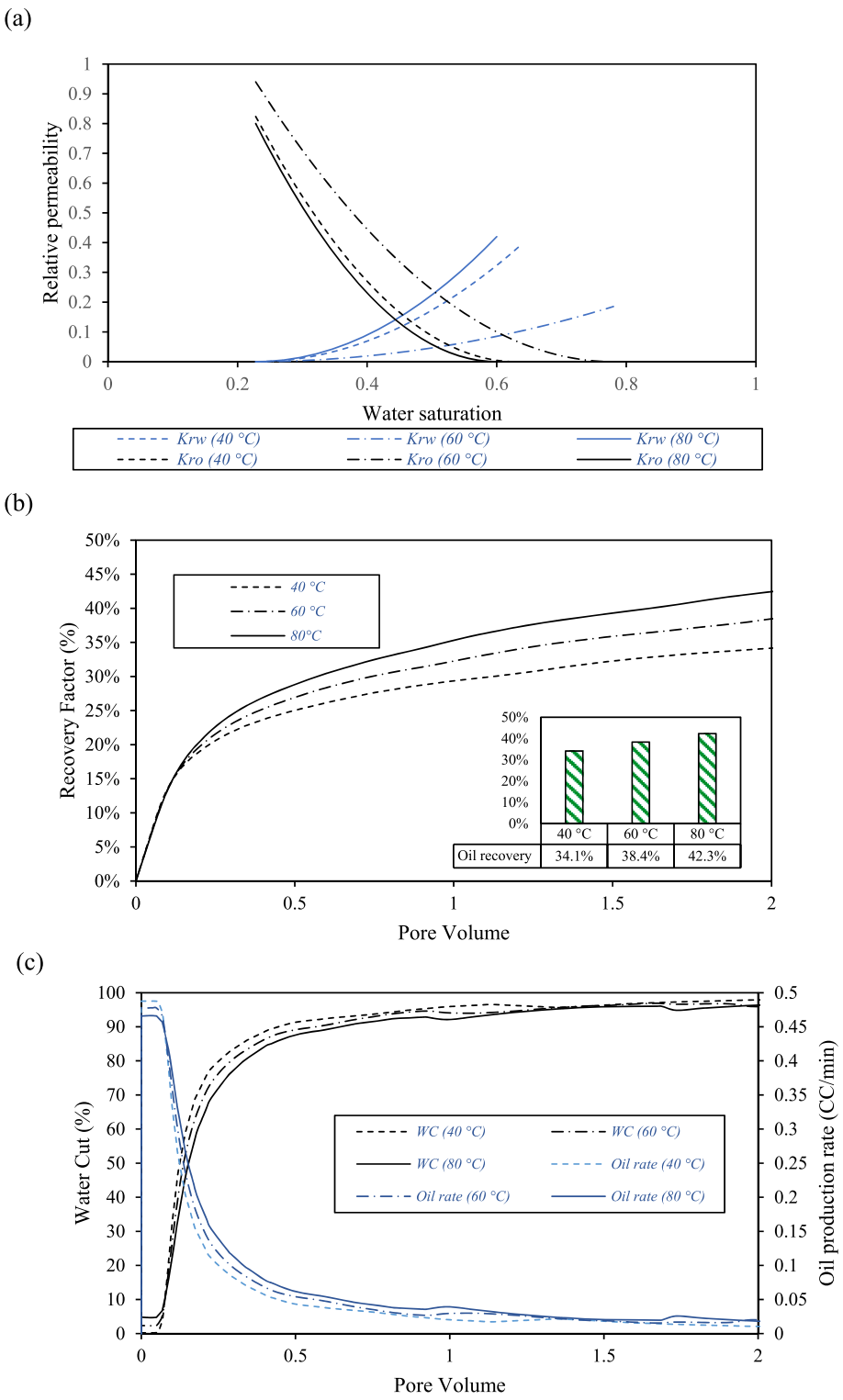

Fig. 15. (a) Relative permeability curves (adjusted for temperature using MEB based on history matched curves to results from Nasralla et al. (2013)), (b) oil recovery profile and (c) oil production and water cut profiles for 40, 60 and 80 °C waterflooding cases.

in the polymer slug viscosity. Hence, the rise in temperature results in making the reservoir wettability more water-wet resulting in higher oil production. The elevated temperature also causes the polymer slug viscosity to drop. However, within the studied range the temperature effect was always positive on the overall low salinity polymer flooding process. Nonetheless, it is expected that there exists a temperature above which the oil recovery will decrease with the increase in temperature due to the thermal degradation of the injection polymer solution. To further investigate the temperature's effect on LSP, the oil production rate and water cut results in Fig. 19c are evaluated.

In conclusion, the oil recovery expected from LSP in a sandstone reservoir is dictated by reservoir temperature. The temperature affects the wettability alteration favourably and the polymer slug viscosity unfavourably, the temperature effect on the wettability is more pronounced. However, is it expected that there exists a temperature above which any increase in the temperature would result in a drop in oil

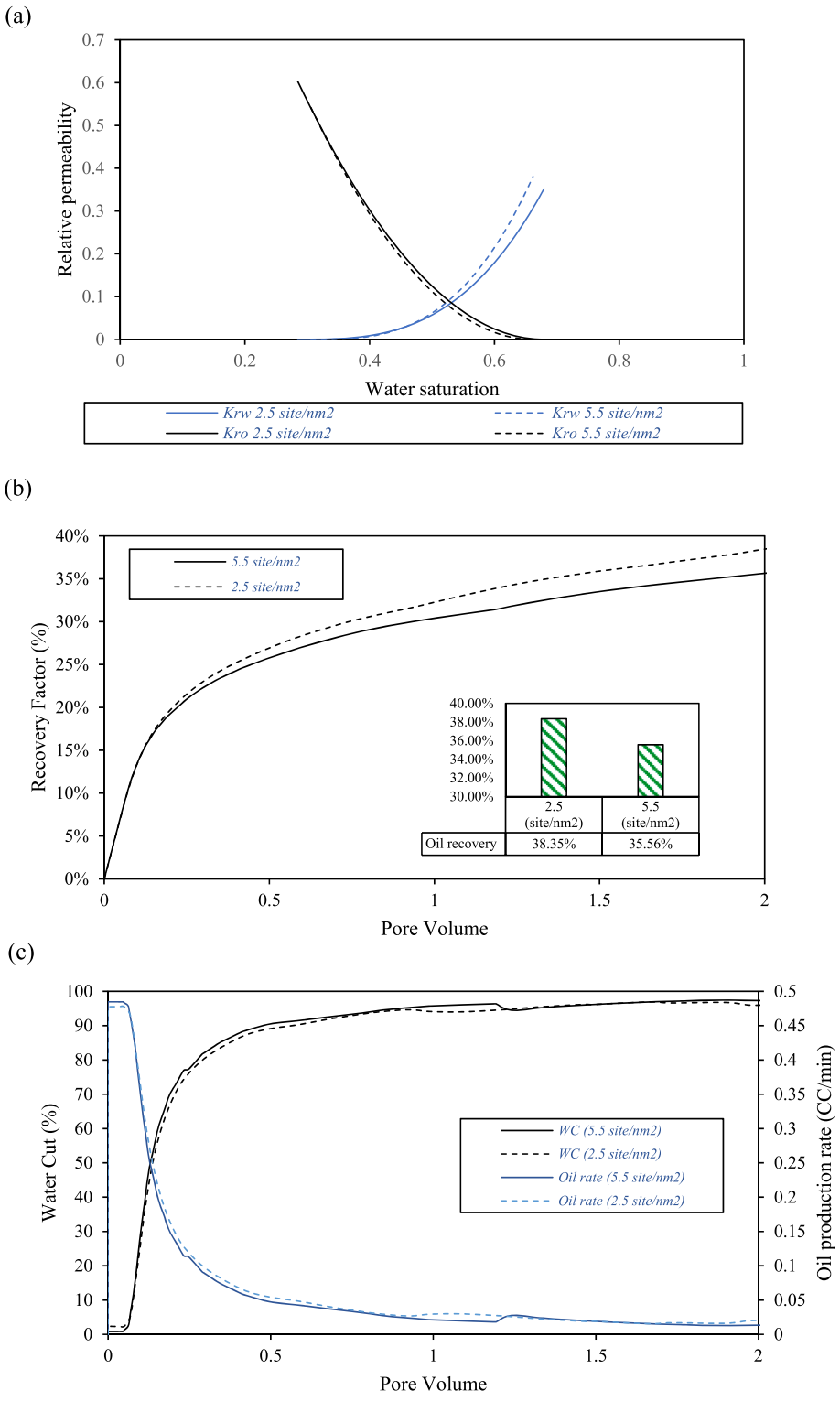

Fig. 16. (a) Relative permeability curves (adjusted for average rock site density using MEB based on history matched curves to results from Nasralla et al. (2013)), (b) oil recovery profile and (c) oil production and water cut profiles for 2.5 and 5.5 site/nm^2 average rock site density cases.

recovery. Above that temperature, the system's wettability remains the same without noticeable change, but the polymer solution viscosity continues to decrease as a result of thermal degradation. This would consequently lead to a reduction in the expected oil recovery from the combined LSP beyond that critical temperature.

3.4.3. *Effect of process type*

In this section, the results of comparing the performances of four types of processes are presented. These processes are high salinity waterflooding, low-salinity waterflooding, high salinity polymer flooding and low-salinity polymer flooding. Each of the two simulated polymer flooding processes consists of 1.2 PV pre-flush water, 0.2 PV polymer slug and 0.6 PV chase water. The oil recovery expected from

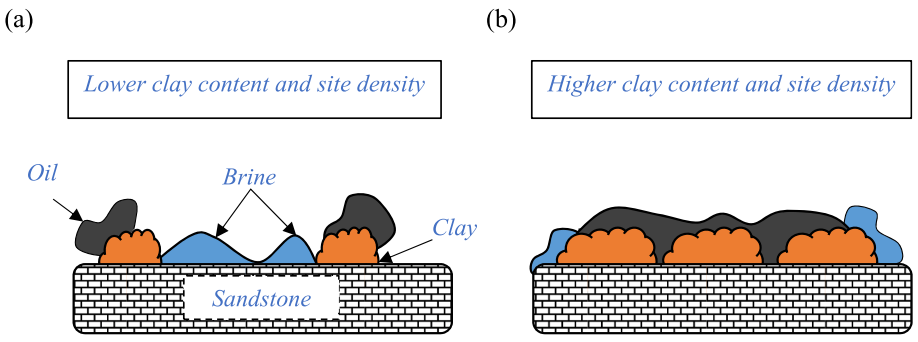

Fig. 17. Representation of oil adhesion to sandstone rock at (a) low clay content and (b) high clay content.

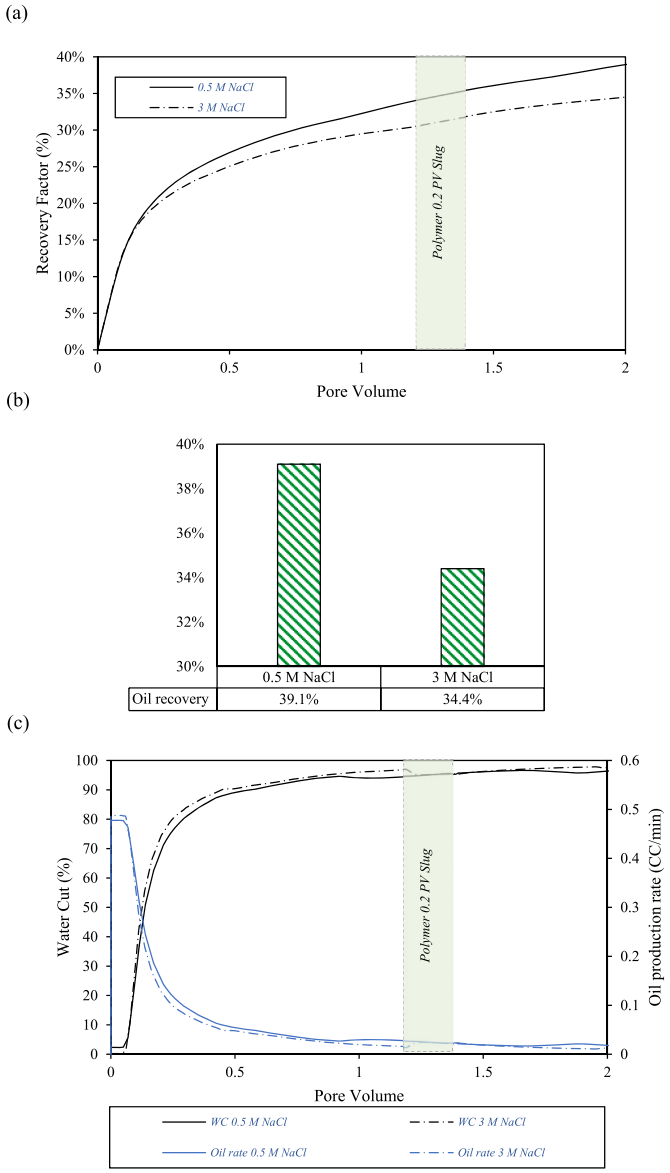

Fig. 18. (a) Oil recovery profile, (b) oil recovery column chart and (c) oil production and water cut profiles for 0.5, 1 and 3 M NaCl polymer flooding cases.

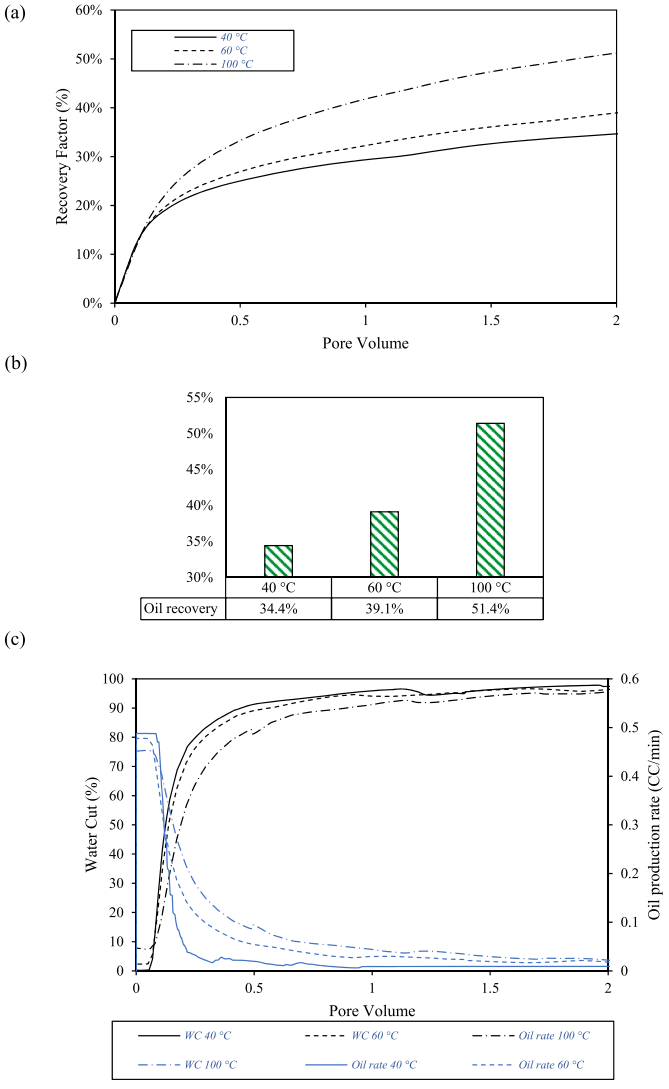

Fig. 19. (a) Oil recovery profile, (b) oil recovery column chart and (c) oil production and water cut profiles for 40, 60 and 100 °C polymer flooding cases.

each process is shown in Fig. 20a and b. The oil recovery expected from the low-salinity polymer flooding is most at 39.1% followed by low-salinity waterflooding which gave 38.4%, high salinity polymer flooding with 34.4% and the least oil recovery is 34.1% from high salinity waterflooding. A comparison of the oil production and water cut expected from each process is shown in Fig. 20c. It is evident that the oil production for each case follows the same order of the oil recovery, where the low-salinity polymer flooding showed the high oil production and the high salinity waterflooding showed the lowest recovery. The trend of the water cut is the opposite of the oil production such that low-salinity polymer flooding shows the lowest overall water cut followed by low-salinity waterflooding, high salinity polymer flooding and high

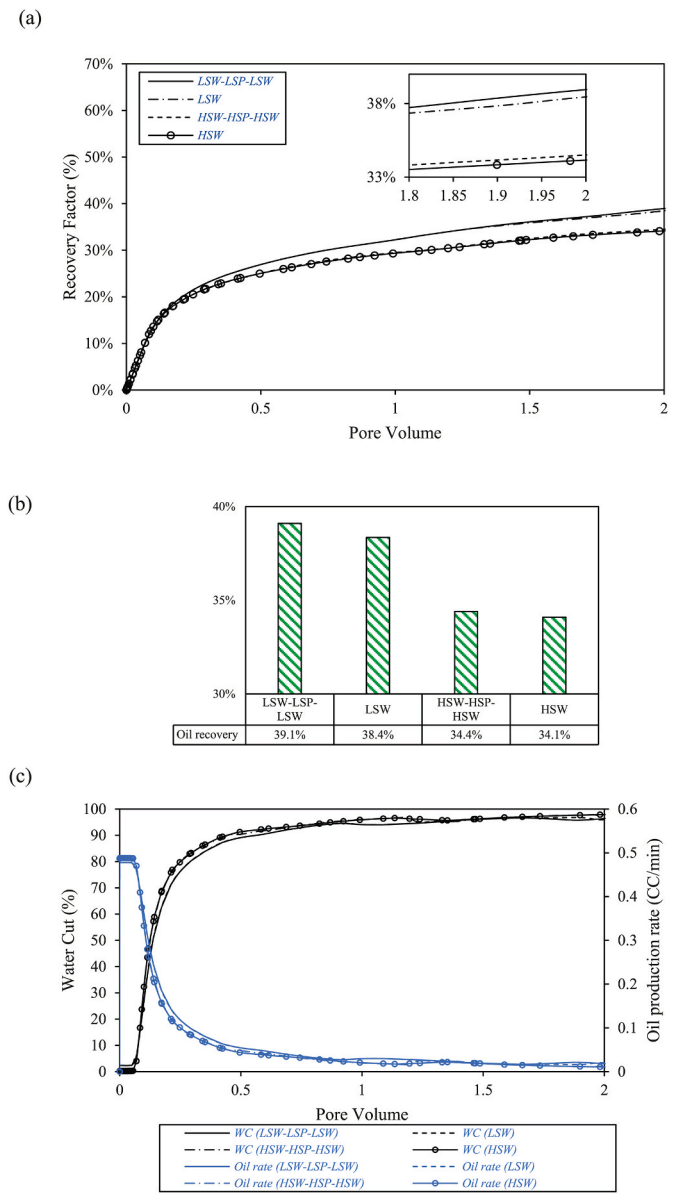

Fig. 20. (a) Oil recovery profile, (b) oil recovery column chart and (c) oil production and water cut profiles for (i) low-salinity polymer flooding (LSW-LSP-LSW), (ii) low-salinity waterflooding (LSW), (iii) high salinity polymer flooding (HSW-HSP-HSW) and high salinity polymer flooding (HSP).

salinity waterflooding.

The comparison presented in Fig. 20b indicates that the low-salinity polymer flooding process results in the highest oil recovery expected compared to the other studied cases. This is due to the fact that the low-salinity polymer flooding process utilises both wettability alteration and improved mobility control due to the improved viscosity of the polymer slug. However, the more interesting finding is that low-salinity water flooding resulted in significantly more oil recovery compared to high salinity polymer flooding. This suggests that low salinity waterflooding in some sandstone reservoirs would be more suited than the standard polymer flooding. Further economic cost-benefit analysis might reveal that low-salinity waterflooding should always be considered before polymer flooding. However, this conclusion is currently applicable to the currently studied reservoir which has a considerably high heterogeneity.

4. Conclusion

In this work, surface complexation modelling and numerical simulation techniques were utilised to investigate various parametric effects on low-salinity waterflooding and low-salinity polymer flooding. Surface complexation modelling was carried out using PHREEQC while the numerical simulation was conducted by employing the multiphase flow simulator CMG-STARS. A hypothetical 3D core model was constructed and used to evaluate the impact of salinity, temperature, pH and rock mineralogy on waterflooding performance. A 3D reservoir section was constructed to analyse the effects of salinity, temperature, rock mineralogy and type of process on the performance of low-salinity water and polymer flooding. Analysis of the results revealed the following conclusions:

1. Reducing the salinity of the injection fluid improved the oil recovery expected from both water flooding and polymer flooding. Low-salinity polymer flooding gave the highest expected oil recovery compared to high salinity polymer flooding and pure waterflooding. This increase in the oil recovery is attributed to the synergetic effects of wettability alteration from low-salinity waterflooding and mobility control due to polymer flooding.
2. A reduction in the clay content positively affected the oil recovery expected from low-salinity waterflooding and low-salinity polymer flooding. The increasing temperature had a favourable effect on wettability alteration and a negative effect on polymer viscosity. A rise in temperature resulted in shifting the reservoir wettability towards more water-wet conditions resulting in more oil recovery. It also resulted in a reduction in the polymer slug viscosity reducing the oil recovery expected from a polymer flooding process. However, an overall positive effect of temperature was observed on the combined low salinity and polymer flooding process within the studied range between 40 and 100 °C.
3. Comparison between studied injection processes i.e., low and high salinity waterflooding, and low and high salinity polymer flooding, revealed that oil recovery as a result of wettability alteration is significantly higher than that of mobility control. Consequently, low-salinity fluids should always be considered for waterflooding and polymer flooding processes.
4. Application of MEB as an interpolation parameter in the relative permeability during the dynamic flooding has been successfully validated and implemented, thus allowing to upscale the interfacial SCM effects at the nano-scale to the macro-scale coreflooding. We believe this this approach is equally applicable for the evaluation of the field-scale recoveries using MEB as an interpolation parameter.

Credit authors statement

Prashant Jadhawar: Writing – original draft, Supervision, Conceptualization, Visualization, Investigation, Methodology, Software, Data curation, Writing – review & editing, Formal analysis. **Motaz Saeed**: Writing – original draft, Visualization, Investigation, Methodology, Software, Data curation, Formal analysis.

Declaration of competing interest

The authors declare that they have no known competing financial interests or personal relationships that could have appeared to influence the work reported in this paper.

Data availability

Data will be made available on request.

Acknowledgement

The authors gratefully acknowledge the valuable support provided by the Computer Modelling Group (CMG), Canada Limited in this study.

9 Appendix A

The brine, oil and rock properties, reservoir conditions, predicted zeta potential, maximum energy barrier and interpolated relative permeability curves for each simulated LSWF and LSP case are shown in Table A1 and Table A2, respectively.

Table A1
Input, predicted zeta potential, calculated MEB and interpolated relative permeability curve for each LSWF case

Case	Input						PhreeqC Output		DLVO	Rel Perm Interpolation			
	Salinity (M)	pH	Temperature (°C)	Avg. rock site density (site/nm^2)	TAN	TBN	OB zeta potential (mV)	RB zeta potential (mV)	MEB	S_{wirr}	S_{or}	Endpoint K_{ro}	Endpoint K_{rw}
1	0.5 NaCl	7	60	2.5	0.5	0.5	−30	−30	0.47	0.2847	0.3206	0.6030	0.3517
2	1 NaCl	7	60	2.5	0.5	0.5	−15	−14	−0.0062	0.3193	0.3494	0.5021	0.3990
3	3 NaCl	7	60	2.5	0.5	0.5	−5	−5	−0.0197	0.3200	0.3500	0.5000	0.4000
4	0.5 $CaCl_2$	7	60	2.5	0.5	0.5	1	1	−0.0129	0.3198	0.3498	0.5007	0.3997
5	1 $CaCl_2$	7	60	2.5	0.5	0.5	9	5	−0.0153	0.3200	0.3500	0.5000	0.4000
6	0.5 NaCl	7	40	2.5	0.5	0.5	−12	−6	−0.0166	0.2280	0.3500	0.5000	0.4000
7	0.5 NaCl	7	60	2.5	0.5	0.5	−30	−30	0.47	0.2847	0.3206	0.6030	0.3517
8	0.5 NaCl	7	80	2.5	0.5	0.5	−38	−32	0.9	0.2534	0.2945	0.6942	0.309
9	1 NaCl	7	60	2.5	0.5	0.5	−30	−30	0.0905	0.2847	0.3206	0.6030	0.3517
10	1 NaCl	7	60	5.5	0.5	0.5	−21	−8	−0.0127	0.3058	0.3381	0.5416	0.3805

Table A2
Input, predicted zeta potential, calculated MEB and interpolated relative permeability curve for each LSP case.

Case	Input								PhreeqC Output		DLVO	Rel Perm Interpolation			
	Salinity (M)	pH	Temperature (°C)	Avg. rock site density (site/nm^2)	TAN	TBN	Polymer Conc. (ppm)	Polymer viscosity (cP)	RB zeta potential (mV)	OB zeta potential (mV)	MEB	S_{wirr}	S_{or}	Endpoint K_{ro}	Endpoint K_{rw}
11	0.5 NaCl	7	60	2.5	0.5	0.5	500	7	−32	−27	0.47	0.28	0.321	0.603	0.352
12	1 NaCl	7	60	2.5	0.5	0.5	500	3.3	−15	−14	−0.0062	0.32	0.349	0.502	0.399
13	3 NaCl	7	60	2.5	0.5	0.5	500	3	−5	−5	−0.0197	0.32	0.35	0.500	0.400
14	0.5 NaCl	7	40	2.5	0.5	0.5	500	0.1	−21	−12	−0.0166	0.32	0.35	0.500	0.400
15	0.5 NaCl	7	60	2.5	0.5	0.5	500	7	−32	−27	0.47	0.28	0.321	0.603	0.352
16	0.5 NaCl	7	100	2.5	0.5	0.5	500	6	−50	−30	1.97	0.23	0.22	0.940	0.180
17	0.5 NaCl	7	60	2.5	0.5	0.5	0	–	−32	−27	0.47	0.28	0.321	0.603	0.352
18	3 NaCl	7	60	2.5	0.5	0.5	500	3	−5	−5	−0.0197	0.32	0.35	0.500	0.400
19	0.5 NaCl	7	60	2.5	0.5	0.5	0	–	−32	−27	0.47	0.28	0.321	0.603	0.352
20	3 NaCl	7	60	2.5	0.5	0.5	0	–	−5	−5	−0.0197	0.32	0.35	0.500	0.400

References

Abdulla, F., Hashem, H.S., Abdulraheem, B., Al-Naqi, M., Al-Qattan, A., John, H., Cunningham, P., Briggs, P., Thawer, R., 2013. First Eor Trial Using Low Salinity Water Injection in the Greater Burgan Field. kuwait.

Al-Sawafi, M.S.M., 2015. No Title, Simulation of Enhanced Heavy Oil Recovery: History Match of Waterflooding and Polymer Injection at Adverse Mobility Ratio.

Alagic, E., Skauge, A., 2010. Combined low salinity brine injection and surfactant flooding in mixed– wet sandstone cores. Energy Fuel. 24, 3551–3559.

Almansour, A.O., AlQuraishi, A.A., AlHussinan, S.N., AlYami, H.Q., 2017. Efficiency of enhanced oil recovery using polymer-augmented low salinity flooding. J. Pet. Explor. Prod. Technol. 7, 1149–1158.

Alotaibi, M.B., Nasralla, R.A., Nasr-El-Din, H.A., 2011. Wettability studies using low-salinity water in sandstone reservoirs. SPE Reservoir Eval. Eng. 14, 713–725.

AlSofi, A.M., Wang, J., AlBoqmi, A.M., AlOtaibi, M.B., Ayirala, S.C., AlYousef, A.A., 2016. SmartWater Synergy with Chemical EOR for a Slightly Viscous Arabian Heavy Reservoir.

Ashraf, A., Hadia, N., Torsaeter, O., Tweheyo, M.T., 2010. Laboratory Investigation of Low Salinity Waterflooding as Secondary Recovery Process: Effect of Wettability.

Austad, T., 2013. Water-based EOR in carbonates and sandstones: new chemical understanding of the EOR potential using "smart water". In: Anonymous Enhanced Oil Recovery Field Case Studies. Elsevier, pp. 301–335.

Awolayo, A.N., Sarma, H.K., Nghiem, L.X., 2018. Modeling the characteristic thermodynamic interplay between potential determining ions during brine-dependent recovery process in carbonate rocks. Fuel 224, 701–717.

Ayirala, S.C., Yousef, A.A., Li, Z., Xu, Z., 2018. Coalescence of crude oil droplets in brine systems: effect of individual electrolytes. Energy Fuel. 32, 5763–5771.

Barkved, O., Heavey, P., Kjelstadli, R., Kleppan, T., Kristiansen, T.G., 2003. Valhall Field-Still on Plateau after 20 Years of Production.

Bonto, M., Eftekhari, A.A., Nick, H.M., 2020. Wettability indicator parameter based on the thermodynamic modeling of chalk-oil-brine systems. Energy Fuel. 34, 8018–8036.

Brady, P.V., Krumhansl, J.L., 2012. A surface complexation model of oil–brine–sandstone interfaces at 100 C: Low salinity waterflooding. J. Petrol. Sci. Eng. 81, 171–176.

Brady, P.V., Morrow, N.R., Fogden, A., Deniz, V., Loahardjo, N., 2015. Electrostatics and the low salinity effect in sandstone reservoirs. Energy Fuel. 29, 666–677.

Buckley, J., Morrow, N., 2010. Improved Oil Recovery by Low Salinity Waterflooding: A Mechanistic Review, pp. 6–9.

Buckley, J., Takamura, K., Morrow, N., 1989. Influence of electrical surface charges on the wetting properties of crude oils. SPE Reservoir Eng. 4, 332–340.

Chen, Y., Xie, Q., Saeedi, A., 2019. Role of ion exchange, surface complexation, and albite dissolution in low salinity water flooding in sandstone. J. Petrol. Sci. Eng. 176, 126–131.

Cissokho, M., Bertin, H., Boussour, S., Cordier, P., Hamon, G., 2010. Low salinity oil recovery on clayey sandstone: experimental study. Petrophysics-The SPWLA Journal of Formation Evaluation and Reservoir Description 51.

CMG, STARS User Manual, (2017).

Dang, C., Nghiem, L., Fedutenko, E., Gorucu, E., Yang, C., Mirzabozorg, A., 2018. Application of Artificial Intelligence for Mechanistic Modeling and Probabilistic Forecasting of Hybrid Low Salinity Chemical Flooding.
Erzuah, S., Fjelde, I., Omekeh, A.V., 2017. Wettability Estimation by Surface Complexation Simulations.
Farooq, U., Tweheyo, M.T., Sjöblom, J., Øye, G., 2011. Surface characterization of model, outcrop, and reservoir samples in low salinity aqueous solutions. J. Dispersion Sci. Technol. 32, 519–531.
Green, D.W., Willhite, G.P., 1998. Enhanced Oil Recovery. Henry L. Doherty Memorial Fund of AIME, Society of Petroleum Engineers.
Gregory, J., 1981. Approximate expressions for retarded van der Waals interaction. J. Colloid Interface Sci. 83, 138–145.
Griffin, T.A., Best, K.D., Thingvoll, T.T., Stockden, I.L., Tjetland, G., 2007. Monitoring Waterflood Performance in a Depleted Fractured Chalk Reservoir.
Hirasaki, G., 1991. Wettability: fundamentals and surface forces, SPE Form. Evaluation 6, 217–226.
Israelachvili, J.N., 2015. Intermolecular and Surface Forces. Academic press.
Jackson, M., Vinogradov, J., Hamon, G., Chamerois, M., 2016a. Evidence, mechanisms and improved understanding of controlled salinity waterflooding part 1: Sandstones. Fuel 185, 772–793.
Jackson, M.D., Al-Mahrouqi, D., Vinogradov, J., 2016b. Zeta potential in oil-water-carbonate systems and its impact on oil recovery during controlled salinity water-flooding. Sci. Rep. 6, 1–13.
Jadhunandan, P., Morrow, N., 1991. Spontaneous imbibition of water by crude oil/brine/rock systems. Situ 15.
Jadhunandan, P., Morrow, N.R., 1995. Effect of wettability on waterflood recovery for crude-oil/brine/rock systems. SPE Reservoir Eng. 10, 40–46.
Jerauld, G.R., Webb, K.J., Lin, C., Seccombe, J.C., 2008. Modeling low-salinity waterflooding. SPE Reservoir Eval. Eng. 11, 1000–1012.
Kamal, M.S., Sultan, A.S., Al-Mubaiyedh, U.A., Hussein, I.A., 2015. Review on polymer flooding: rheology, adsorption, stability, and field applications of various polymer systems. Polym. Rev. 55, 491–530.
Khaledialidusti, R., Kleppe, J., 2018. Surface-charge alteration at the carbonate/brine interface during single-well chemical-tracer tests: surface-complexation model. SPE J. 23, 2302–2315.
Khorsandi, S., Qiao, C., Johns, R.T., Torrealba, V.A., 2016. Simulation of Surfactant-Polymer Floods with a Novel Microemulsion Equation of State.
Khorsandi, S., Qiao, C., Johns, R.T., 2017. Displacement efficiency for low-salinity polymer flooding including wettability alteration. SPE J. 22, 417–430.
Kolltveit, Y., 2016. Relationship between Crude Oil Composition and Physical-Chemical Properties.
Korrani, A.K., Jerauld, G.R., Sepehrnoori, K., 2016. Mechanistic modeling of low-salinity waterflooding through coupling a geochemical package with a compositional reservoir simulator. SPE Reservoir Eval. Eng. 19, 142–162.
Kozaki, C., 2012. Efficiency of Low Salinity Polymer Flooding in Sandstone Cores.
Lager, A., Webb, K., Black, C., 2007. Impact of Brine Chemistry on Oil Recovery cp-24.
Lager, A., Webb, K.J., Black, C., Singleton, M., Sorbie, K.S., 2008. Low salinity oil recovery-an experimental investigation 1. Petrophysics-The SPWLA Journal of Formation Evaluation and Reservoir Description 49.
Lebedeva, E.V., Fogden, A., 2010. Adhesion of oil to kaolinite in water. Environ. Sci. Technol. 44, 9470–9475.
Lee, S., Kim, D.H., Huh, C., Pope, G.A., 2009. Development of a Comprehensive Rheological Property Database for EOR Polymers.
Lee, K.E., Khan, I., Morad, N., Teng, T.T., Poh, B.T., 2012. Physicochemical and rheological properties of novel magnesium salt-polyacrylamide composite polymers. J. Dispersion Sci. Technol. 33, 1284–1291.
Ligthelm, D.J., Gronsveld, J., Hofman, J., Brussee, N., Marcelis, F., van der Linde, H., 2009. Novel Waterflooding Strategy by Manipulation of Injection Brine Composition.
Liu, F., Wang, M., 2021. Electrokinetic Mechanisms and Synergistic Effect on Ion-Tuned Wettability in Oil-Brine-Rock Systems. Transp. Porous Media, pp. 1–20.
Luo, J., Liu, Y., Zhu, P., 2006. In: Shen, P.-P., Liu, Y.-Z., Liu, H.-R. (Eds.), Polymer Solution Properties and Displacement Mechanisms, Enhanced Oil Recovery-Polymer Flooding, pp. 1–72.
Mandal, A., Ojha, K., 2008. Optimum Formulation of Alkaline-Surfactant-Polymer Systems for Enhanced Oil Recovery.
McGuire, P., Chatham, J., Paskvan, F., Sommer, D., Carini, F., 2005. Low Salinity Oil Recovery: an Exciting New EOR Opportunity for Alaska's North Slope.
Mohammadi, H., Jerauld, G.R., 2012. Mechanistic Modeling of the Benefit of Combining Polymer with Low Salinity Water for Enhanced Oil Recovery.
Morrow, N.R., 1990. Wettability and its effect on oil recovery. J. Petrol. Technol. 42, 1476–1484.
Nasralla, R.A., Nasr-El-Din, H.A., 2014. Double-layer expansion: is it a primary mechanism of improved oil recovery by low-salinity waterflooding? SPE Reservoir Eval. Eng. 17, 49–59.
Nasralla, R.A., Bataweel, M.A., Nasr-El-Din, H.A., 2013. Investigation of wettability alteration and oil-recovery improvement by low-salinity water in sandstone rock. J. Can. Pet. Technol. 52, 144–154.
Nicolini, J.V., Ferraz, H.C., Borges, C.P., 2017. Effect of seawater ionic composition modified by nanofiltration on enhanced oil recovery in Berea sandstone. Fuel 203, 222–232.
Norris, U.L., 2011. No Title, Core-Scale Simulation of Polymer Flow through Porous Media.
Omekeh, A.V., Evje, S., Friis, H.A., 2012. Modeling of low salinity effects in sandstone oil rocks. Int. J. Numer. Anal. Model. 1, 1–18.
Pooryousefy, E., Xie, Q., Chen, Y., Sari, A., Saeedi, A., 2018. Drivers of low salinity effect in sandstone reservoirs. J. Mol. Liq. 250, 396–403.
Qiao, C., Johns, R., Li, L., 2016. Modeling low-salinity waterflooding in chalk and limestone reservoirs. Energy Fuel. 30, 884–895.
RezaeiDoust, A., Puntervold, T., Austad, T., 2010. A Discussion of the Low Salinity EOR Potential for a North Sea Sandstone Field.
Rivet, S.M., Lake, L.W., Pope, G.A., 2010. A Coreflood Investigation of Low-Salinity Enhanced Oil Recovery.
Robertson, E.P., 2007a. Low-salinity Waterflooding to Improve Oil Recovery-Historical Field Evidence.
Robertson, E.P., 2007b. Low-salinity Waterflooding to Improve Oil Recovery-Historical Field Evidence.
Sadeqi-Moqadam, M., Riahi, S., Bahramian, A., 2016. An investigation into the electrical behavior of oil/water/reservoir rock interfaces: the implication for improvement in wettability prediction. Colloids Surf. Physicochem. Eng. Aspects 490, 268–282.
Saeed, M., Jadhawar, P., Ayirala, S.C., Abhishek, R., Zhou, Y., 2022a. Modelling the effects of reservoir parameters and rock mineralogy on wettability during low salinity waterflooding in sandstone reservoirs. J. Petrol. Sci. Eng., 110676
Saeed, M., Jadhawar, P., Zhou, Y., Abhishek, R., 2022b. Triple-layer surface complexation modelling: characterization of oil-brine interfacial zeta potential under varying conditions of temperature, pH, oil properties and potential determining ions. Colloids Surf. Physicochem. Eng. Aspects. 633, 127903.
SayedAkram, N.I., Mamora, D., 2011. Simulation Study on Surfactant-Polymer Flood Performance in Fractured Carbonate Reservoir.
Seccombe, J.C., Lager, A., Webb, K.J., Jerauld, G., Fueg, E., 2008. Improving Wateflood Recovery: LoSalTM EOR Field Evaluation.
Shaker Shiran, B., Skauge, A., 2013. Enhanced oil recovery (EOR) by combined low salinity water/polymer flooding. Energy Fuel. 27, 1223–1235.
Sharma, M., Filoco, P., 2000. Effect of brine salinity and crude-oil properties on oil recovery and residual saturations. SPE J. 5, 293–300.
Sharma, H., Mohanty, K.K., 2018. An experimental and modeling study to investigate brine-rock interactions during low salinity water flooding in carbonates. J. Petrol. Sci. Eng. 165, 1021–1039.
Sheng, J., 2010. Modern Chemical EOR-Theory and Practice.
Skrettingland, K., Holt, T., Tweheyo, M.T., Skjevrak, I., 2011. Snorre low-salinity-water injection—coreflooding experiments and single-well field pilot. SPE Reservoir Eval. Eng. 14, 182–192.
Sohrabi, M., Mahzari, P., Farzaneh, S.A., Mills, J.R., Tsolis, P., Ireland, S., 2017. Novel insights into mechanisms of oil recovery by use of low-salinity-water injection. SPE J. 22, 407–416.
Taheriotaghsara, M., Bonto, M., Nick, H.M., Eftekhari, A.A., 2021. Estimation of calcite wettability using surface forces. J. Ind. Eng. Chem. 98, 444–457.
Tahir, M., Hincapie, R.E., Foedisch, H., Abdullah, H., Ganzer, L., 2018. Impact of Sulphates Presence during Application of Smart Water Flooding Combined with Polymer Flooding.
Takeya, M., Shimokawara, M., Elakneswaran, Y., Nawa, T., Takahashi, S., 2019a. Predicting the electrokinetic properties of the crude oil/brine interface for enhanced oil recovery in low salinity water flooding. Fuel 235, 822–831.
Takeya, M., Shimokawara, M., Elakneswaran, Y., Okano, H., Nawa, T., 2019b. Effect of acid number on the electrokinetic properties of crude oil during low-salinity waterflooding. Energy Fuel. 33, 4211–4218.
Tam, K., Tiu, C., 1990. Role of ionic species and valency on the steady shear behavior of partially hydrolyzed polyacrylamide solutions. Colloid Polym. Sci. 268, 911–920.
Tang, G., Morrow, N.R., 1997. Salinity, temperature, oil composition, and oil recovery by waterflooding. SPE Reservoir Eng. 12, 269–276.
Tang, G., Morrow, N.R., 1999. Influence of brine composition and fines migration on crude oil/brine/rock interactions and oil recovery. J. Petrol. Sci. Eng. 24, 99–111.
Tetteh, J.T., Cudjoe, S.E., Aryana, S.A., Ghahfarokhi, R.B., 2021. Investigation into fluid-fluid interaction phenomena during low salinity waterflooding using a reservoir-on-a-chip microfluidic model. J. Petrol. Sci. Eng. 196, 108074.
Tetteh, J.T., Pham, A., Peltier, E., Hutchison, J.M., Ghahfarokhi, R.B., 2022a. Predicting the electrokinetic properties on an outcrop and reservoir composite carbonate surfaces in modified salinity brines using extended surface complexation models. Fuel 309, 122078.
Tetteh, J.T., Barimah, R., Korsah, P.K., 2022b. Ionic interactions at the crude oil–brine–rock interfaces using different surface complexation models and DLVO theory: application to carbonate wettability. ACS Omega 7, 7199–7212.
Torrijos, I.D.P., Puntervold, T., Strand, S., Austad, T., Bleivik, T.H., Abdullah, H.I., 2018. An experimental study of the low salinity Smart Water-Polymer hybrid EOR effect in sandstone material. J. Petrol. Sci. Eng. 164, 219–229.
Tunnish, A., Shirif, E., Henni, A., 2019. History matching of experimental and CMG-STARS results. J. Pet. Explor. Prod. Technol. 9, 341–351.
Unsal, E., Ten Berge, A., Wever, D., 2018. Low salinity polymer flooding: lower polymer retention and improved injectivity. J. Petrol. Sci. Eng. 163, 671–682.
Vledder, P., Fonseca, J.C., Wells, T., Gonzalez, I., Ligthelm, D., 2010. Low Salinity Water Flooding: Proof of Wettability Alteration on a Field Wide Scale.
Webb, K., Black, C.a., Al-Ajeel, H., 2004. Low Salinity Oil Recovery-Log-Inject-Log.
Webb, K., Black, C., Edmonds, I., 2005. Low Salinity Oil Recovery–The Role of Reservoir Condition Corefloods cp-12.
Wu, Y., Bai, B., 2009. Efficient Simulation for Low Salinity Waterflooding in Porous and Fractured Reservoirs.
Xie, Q., Liu, Y., Wu, J., Liu, Q., 2014. Ions tuning water flooding experiments and interpretation by thermodynamics of wettability. J. Petrol. Sci. Eng. 124, 350–358.
Xie, Q., Brady, P.V., Pooryousefy, E., Zhou, D., Liu, Y., Saeedi, A., 2017. The low salinity effect at high temperatures. Fuel 200, 419–426.

Yang, J., Dong, Z., Dong, M., Yang, Z., Lin, M., Zhang, J., Chen, C., 2016. Wettability alteration during low-salinity waterflooding and the relevance of divalent ions in this process. Energy Fuel. 30, 72–79.
Yildiz, H.O., Morrow, N.R., 1996. Effect of brine composition on recovery of Moutray crude oil by waterflooding. J. Petrol. Sci. Eng. 14, 159–168.
Yousef, A.A., Liu, J., Blanchard, G., Al-Saleh, S., Al-Zahrani, T., Al-Zahrani, R., Al-Tammar, H., Al-Mulhim, N., 2012. Smartwater Flooding: Industry's First Field Test in Carbonate Reservoirs.
Zhang, Y., Morrow, N.R., 2006. Comparison of Secondary and Tertiary Recovery with Change in Injection Brine Composition for Crude-Oil/sandstone Combinations.
Zhang, Y., Xie, X., Morrow, N.R., 2007a. Waterflood Performance by Injection of Brine with Different Salinity for Reservoir Cores.
Zhang, P., Tweheyo, M.T., Austad, T., 2007b. Wettability alteration and improved oil recovery by spontaneous imbibition of seawater into chalk: impact of the potential determining ions Ca2 , Mg2 , and SO42. Colloids Surf. Physicochem. Eng. Aspects 301, 199–208.